Research Article

Pathogenic neutrophilia drives acute respiratory distress syndrome in severe COVID-19 patients

Running title: Pathogenic neutrophilia in severe COVID-19

Devon J. Eddins[1,2,3], Junkai Yang[1,9], Astrid Kosters[1,9], Vincent D. Giacalone[2,4], Ximo Pechuan[5], Joshua D. Chandler[2,4], Jinyoung Eum[1,6], Benjamin R. Babcock[1], Brian S. Dobosh[2,4], Mindy R. Hernández[7], Fathma Abdulkhader[1], Genoah L. Collins[2,4], Richard P. Ramonell[7], Christine Moussion[5], Darya Y. Orlova[5], Ignacio Sanz[1,3,8], F. Eun-Hyung Lee[1,3,7], Rabindra M. Tirouvanziam[2,4], Eliver E.B. Ghosn[1,2,3,6*]

[1]Lowance Center for Human Immunology, Department of Medicine, Division of Immunology and Rheumatology, Emory University School of Medicine, Atlanta, GA 30322, USA

[2]Department of Pediatrics, Emory University School of Medicine, Atlanta, GA 30322, USA

[3]Emory Vaccine Center, Yerkes National Primate Research Center, Emory University School of Medicine, Atlanta, GA 30322, USA

[4]Center for CF & Airways Disease Research, Children's Healthcare of Atlanta, Atlanta, 30322 GA, USA

[5]Genentech, Inc., South San Francisco, California 94080, USA

[6]Georgia Institute of Technology, Bioinformatics Graduate Program, Atlanta, GA 30332, USA

[7]Division of Pulmonary, Allergy, Critical Care & Sleep Medicine, Department of Medicine, Emory University School of Medicine, Atlanta, GA 30322, USA

[8]Emory Autoimmunity Center of Excellence, Department of Medicine, Division of Rheumatology, Emory University School of Medicine, Atlanta, GA 30322, USA

[9]These authors contributed equally: Junkai Yang and Astrid Kosters

Corresponding Author Contact Info

Eliver E.B. Ghosn (ORCID: 0000-0001-7258-906X): Lowance Center for Human Immunology, Health Sciences Research Building, 1760 Haygood Dr. NE, E240, Atlanta, GA 30322, USA; tel: +1-404-712-3211; email: eliver.ghosn@emory.edu

Abstract

Severe acute respiratory syndrome coronavirus 2 (SARS-CoV-2) and the ensuing COVID-19 pandemic have caused ~40 million cases and over 648,000 deaths in the United States alone. Troubling disparities in COVID-19-associated mortality emerged early, with nearly 70% of deaths confined to Black/African-American (AA) patients in some areas, yet targeted studies within this demographic are scant. Multi-omics single-cell analyses of immune profiles from airways and matching blood samples of Black/AA patients revealed low viral load, yet pronounced and persistent pulmonary neutrophilia with advanced features of cytokine release syndrome and acute respiratory distress syndrome (ARDS), including exacerbated production of IL-8, IL-1β, IL-6, and CCL3/4 along with elevated levels of neutrophil elastase and myeloperoxidase. Circulating S100A12^{+}/IFITM2^{+} mature neutrophils are recruited via the IL-8/CXCR2 axis, which emerges as a potential therapeutic target to reduce pathogenic neutrophilia and constrain ARDS in severe COVID-19.

Introduction

The coronavirus disease 2019 (COVID-19) pandemic, caused by SARS-CoV-2, is associated with high morbidity and mortality. To date, the pandemic has caused ~40 million cases and over 648,000 deaths in the United States alone, where communities of color are disproportionately burdened with disease severity and mortality[1, 2]. A hallmark of COVID-19 pathogenesis is the vast array of clinical presentations and outcomes, ranging from asymptomatic or mild, self-limiting disease to acute respiratory distress syndrome (ARDS), multiorgan failure, and death. Indeed, such diversity in COVID-19 pathogenesis poses challenges to identify processes that dictate progression to severe disease. Early reports highlighted systemic hyperinflammatory responses that are linked to disease severity[3]. Cytokine release syndrome, also called a cytokine storm, has been observed in many patients and is suspected of causing the detrimental progression of COVID-19 and sustained immune dysregulation[4].

Severe COVID-19 parallels the pathophysiology of sepsis[5], where clinical presentation often includes granulocytosis, elevated proinflammatory cytokine production, aberrant myeloid activation, altered dendritic cell (DC) population dynamics, and lymphopenia[6, 7]. Early single-cell analyses of bronchoalveolar lavage fluid (BALF) samples implicated dysregulated monocyte and macrophage responses as central features in poor outcomes[4, 8]. As such, most early efforts have been focused on characterizing and constraining aberrant monocyte/macrophage responses. Concurrently, reports of neutrophilia in the peripheral blood arose, and the neutrophil to lymphocyte ratio emerged as an independent risk factor for disease progression[9]. Interestingly, a prior investigation of ARDS following sepsis identified sustained neutrophilia associated with worsened prognosis and death compared to patients who resolved neutrophilia and showed an increase in tissue-resident alveolar macrophages[10], which may present another shared feature between COVID-19 and sepsis.

To date, there have been many studies of neutrophil responses in the blood of COVID-19 patients[11, 12, 13, 14, 15]. However, an in-depth analysis of the neutrophil activity in the lungs is lacking. Expressly, the extent to which neutrophils contribute to cytokine release syndrome, tissue damage, and ultimately ADRS in severe COVID-19 cases is incompletely understood. Our systems immunology approach, combining high-dimensional (Hi-D, 30-parameter) flow cytometry and multi-omics single-cell sequencing analyses of immune profiles from the airways and matching blood samples of Black/African-American (AA) patients, revealed pronounced and sustained pulmonary neutrophilia as a hallmark of severe disease. Furthermore, mature pulmonary neutrophils produce very high levels of the neutrophil chemotactic factor IL-8 in addition to IL-1β, IL-6, and CCL3/4 along with copious amounts of neutrophil elastase (NE) and myeloperoxidase (MPO). Altogether, our findings highlight that transcriptionally active and highly inflammatory neutrophils are sustained in the airways of severe patients and that reducing pathogenic neutrophilia may constrain ARDS in severe COVID-19 disease.

Results

Study Cohort

To better understand immune dynamics in Black/AA patients with severe COVID-19, we analyzed airway and matching blood samples from a cohort of 35 individuals presenting to Emory University Hospitals (severe) or the Emory Acute Respiratory Clinic (mild-acute) in Atlanta, GA, USA (Fig. 1 and Extended Data Table 1), including 8 demographic-matched healthy adults as controls. Of the 27 individuals who were confirmed positive by PCR from nasopharyngeal swabs, 18 had an NIH severity score of "critical" (https://www.covid19treatmentguidelines.nih.gov/overview/clinical-spectrum/; referred to as severe herein) and were admitted to the intensive care unit (ICU) requiring mechanical ventilator support, and 9 were mild (mild-acute) outpatients. All severe patients in our cohort received corticosteroids (dexamethasone or equivalent). Approximately half received one or more doses of the antiviral medication remdesivir, with an average ICU stay of 26 days (see Extended Data Tables 1 and 2).

Exacerbated neutrophilia in the airways and matching blood of severe COVID-19 patients

We first characterized major immune lineages in the airways (endotracheal aspiration, ETA) and matching blood samples by Hi-D flow cytometry and observed a pronounced circulating neutrophilia and lymphopenia (notably T and NK cells), which is similarly reflected in the airways (Fig. 2a-e and Extended Data Fig. 1). This is in line with recent reports showing lymphopenia associated with significant alterations in the myeloid compartment[15, 16]. Strikingly, in most cases of severe disease, ≥85% of all pulmonary leukocytes were neutrophils (Fig. 2b). This contrasts with other studies that have reported much more heterogeneity in neutrophil frequency in patients' blood and lungs[17, 18]. In addition, circulating T cells and NK cells decline with increased disease severity (Fig. 2d), which has recently been reported as a feature of COVID-19 pneumonia[19]. We also observed a notable decrease in pulmonary NK cells associated with disease severity (Fig. 2b). However, there were only subtle differences in the B-cell compartment (which were detected at very low levels in the airways) and myeloid-derived cells (MdCs) compartment compared to other reports[8, 20, 21], highlighting the importance of neutrophilia and neutrophil-to-lymphocyte ratio in our cohort. Interestingly, the patient with the lowest neutrophil frequency in the airways corresponds to the youngest patient in the severe disease group (Fig. 2b). However, since we only had a single patient under 35 years old in our severe group, we cannot conclude any associations between neutrophilia and patient age.

Since we identified prominent neutrophilia in our cohort, we developed a Hi-D, 30-parameter flow cytometry panel to interrogate inflammatory neutrophil phenotype in addition to broad leukocyte characterization (see "CoV-Neutrophil" panel in Extended Data Table 3). Here, we used extracellular staining of neutrophil elastase (NE) and CD63 (LAMP3) to assess primary granule release[22], coupled with intracellular staining for key effectors implicated in cytokine storm (IL-1β, IL-6, and IL-8). We observed that nearly all neutrophils recruited to the lung developed an inflammatory profile characterized by exacerbated levels of NE and elevated

production of IL-1β and IL-8 with a dramatic increase in primary granule release (Fig. 2c,e). Indeed, most neutrophils in the airways were positive for all 3 intracellular cytokines and express CD63 on the cell surface (Fig. 2c), suggesting that neutrophils are releasing cytokines upon degranulation. However, this phenotype is diminished in the circulation. A smaller proportion of blood neutrophils undergo granule release and express a cytokine signature limited mainly to IL-1β production and less IL-6 and IL-8 (Fig. 2e). Similarly, we find a subset of neutrophils in the lung that co-express the highest levels of surface CD10, CD184 (CXCR4) and NE (Fig. 2c). Interestingly, neutrophils in the lung express lower levels of FcγRII (CD32) than those in the blood (Extended Data Fig. 5a). Together, these results demonstrate systemic neutrophilia in severe COVID-19 patients where neutrophils accumulating in the airways produce exacerbated levels of potentially damaging enzymes (e.g., NE) and inflammatory cytokines (IL-1β/6/8) while undergoing pronounced primary granule release.

Neutrophil-secreted inflammatory molecules in the airways potentiate acute respiratory distress syndrome in severe patients

To better understand the inflammatory signaling milieu and relate the intracellular cytokine staining to protein secretion, we measured 21 total analytes in the airways and plasma using the Mesoscale UPLEX platform (Extended Data Table 4). We found that IL-8 is the most abundant chemokine in the airways of severe patients accompanied by high levels of IL-1β and IL-6. This is in line with our Hi-D flow cytometry data showing neutrophilia and pronounced intracellular staining signal for IL-8 and IL-1β (Fig. 3a-i). Strikingly, IL-8 levels were ~100-fold higher in the airways of severe versus mild patients and that of IL-1β and IL-6 levels in severe patients. These findings are in stark contrast to an early report[23] that showed no differences between circulating and pulmonary IL-6 and IL-8 secretion, reported in the <100 pg/mL range. However, more recent studies in both ETA[24] and BALF[25] samples have noted similar findings that corroborate our own. These data, therefore, implicate IL-8 signaling in the prominent neutrophilia observed in severe patients in our cohort.

We noticed only minor differences in circulating levels of many targets between healthy individuals and those affected by severe COVID-19 disease suggesting an uncoupling of local versus systemic inflammatory responses[24], particularly for IL-8 and IL-1β, but also IL-6 to a lesser extent (Fig. 3a,d,g). Conversely, we observed a rise in circulating IL-1RA levels with increasing disease severity, similar to other reports[26]. However, we observed an opposite trend in the airways, where IL-1RA levels appear to be decreased in severe patients (Fig. 3j). This is in stark contrast to IL-1β levels, which were not markedly different in the circulation but significantly increased in the airways with disease severity (Fig. 3j). We also found increased CCL2 (MCP-1) in the airways of severe disease, and the same trend for M-CSF and TNF was observed, albeit at much lower concentrations (Fig. 3j). Interferon (IFN)-γ was detected at the highest levels in the airways of severe patients with no obvious differentiation in plasma across all groups. IL-10 was also increased in the airways of severe patients with notable variation at low levels (Fig. 3j). In contrast to other studies[27, 28], we did not observe appreciable differences in IL-18 or CXCL10 (IP-10) levels across patient groups (Extended Data Fig. 2). Additionally,

175 CXCL12 was not detected in the airways of patients, and there were no notable differences in
176 plasma levels across patient groups (Extended Data Fig. 2).
177
178 We further measured the concentration of neutrophil-derived MPO and its enzymatic activity
179 across patient groups. MPO is an important neutrophil effector molecule (originating from
180 primary granules like NE) implicated in respiratory illnesses such as cystic fibrosis[29], and can
181 contribute to lung tissue damage during neutrophilic pneumonitis. MPO protein concentrations
182 increased stepwise with disease severity in the plasma and respiratory supernatant (Fig. 3k).
183 However, MPO activity was mostly detected in the airways, and rose with increasing disease
184 severity (Fig. 3k).
185
186 **Recruited airway neutrophils are mature, transcriptionally active, and further differentiate**
187 **into a highly inflammatory state**
188
189 To gain insight into the cellular states and transcriptional regulation in patients with severe
190 COVID-19 disease, we performed multi-omics scRNA-seq on cells from whole blood and ETA
191 samples of severe patients and whole blood from demographic-matched healthy control (Fig. 1).
192 We assessed immune features in data integrated from four or more patients from the same
193 cohort (i.e., healthy vs. severe; see Methods). First, major lineages from blood (Fig. 4a) and
194 ETA (Fig. 4g) were gated manually using the antibody-derived tag (ADT) data for surface
195 protein expression. Next, we used the gene expression (GEX) data to generate clusters for
196 each major lineage identified based on their surface markers, as per our previously described
197 SuPERR-seq pipeline[30] (Extended Data Fig. 3). For example, neutrophils identified by CD66b
198 and CD16 surface ADT in the blood (Fig. 4b) and ETA (Fig. 4h) were then selected and
199 clustered independently by GEX data (Fig. 4c,i) for further analyses.
200
201 A prior study had reported an increase in immature neutrophils in the lung concomitant to
202 increased circulating immature neutrophils from emergency hematopoiesis in severe COVID-19
203 patients[16]. We, therefore, assessed the immature neutrophil phenotype in the blood (Fig 4a-e)
204 and lung (Fig 4f-j) by scRNA-seq in our patient cohort. We readily identified a cluster of
205 neutrophils expressing *CAMP*, *LTF*, *RETN*, *OLFM4*, *DEFA3*, *CD24*, and *MMP8* (Fig. 4e and
206 Extended Data Fig. 4) in the blood of severe patients (cluster 3 in blood neutrophils) that also
207 has high expression of calprotectin (S100A8/9) and other calgranulins (Fig 4d). This is
208 consistent with immature neutrophil phenotypes described by others[7, 15] and was notably absent
209 in neutrophils from healthy blood, confirming an emergency hematopoiesis/granulopoiesis in our
210 patient cohort. However, in contrast to previous studies[16], we did not observe any signature of
211 immature neutrophils in the lungs of severe patients (Fig. 4j), suggesting that immature
212 neutrophils either are not directly recruited to the lung, or quickly differentiate upon infiltration
213 into the lung.
214
215 To determine which neutrophil subset in the blood can infiltrate the lung and further differentiate
216 into a pathogenic state, we explored cell-cell communication (CellChat[31]) of clustered cells from
217 blood (Fig. 4c) and lung (Fig. 4h) samples. We found significant communication through the
218 CXCL pathway between the lung neutrophil, myeloid, and non-immune populations (i.e.,

219 epithelial/stromal cells) with *CXCR2*-expressing neutrophils from the blood (blood cluster 2; Fig.
220 5a). The CXCL8 (IL-8)/CXCR2 pathway was identified as the primary recruitment axis for
221 circulating *CXCR2*$^{+}$ neutrophils (Fig. 5b). These data are in line with our finding that IL-8 was
222 increased in neutrophils by flow cytometry (Fig. 2) and secreted at very high levels in the
223 airways (Fig. 3) and suggests that the CXCL8/CXCR2 signaling axis is important for neutrophil
224 recruitment to the lungs during COVID-19 pathogenesis. Virtually all lung neutrophils
225 (particularly cluster 5), non-immune cells, and monocytes show the potential to recruit
226 circulating neutrophils (Fig. 5a,d), indicating a robust and redundant mechanism of neutrophil
227 recruitment to the airways via the CXCL8/CXCR2 axis. Surprisingly, the immature neutrophils
228 (blood cluster 3) lacked *CXCR2* (Fig. 5c), suggesting that immature neutrophils are unlikely to
229 infiltrate the lung via IL-8. In contrast, a defined subset of mature neutrophils in blood
230 expressing high levels of *CXCR2*, along with interferon-induced *IFITM2* and *S100A11/12*,
231 identify blood cluster 2 as the putative neutrophil subset that can infiltrate the lung via IL-8 (Figs.
232 4d and 5c-d). It is, therefore, probable that recent lung emigrants would still express detectable
233 levels of *CXCR2*, as well as *IFITM2* and *S100A11/12* (Fig. 5c).
234
235 After identifying the blood neutrophil cluster 2 as the putative source of lung-recruited
236 neutrophils, we sought to identify their cell trajectory/differentiation once they enter the inflamed
237 airway. Cell trajectory analyses (scVelo[32]) revealed two differentiation pathways (Trajectories 1
238 and 2) for the recently infiltrated neutrophils (Fig. 5e). Indeed, cells expressing the highest levels
239 of *CXCR2* and *S100A11/12* were at the beginning of the trajectory, further supporting these as
240 the putative emigrant population from the blood (Fig. 5f). Notably, neutrophils recruited to the
241 lung and differentiated along Trajectory 2 experience transcriptional reprogramming to acquire a
242 heightened inflammatory phenotype (Fig. 5e,f). In contrast to the canonical neutrophil
243 differentiation pathway, including a short half-life, the infiltrated neutrophils in severe COVID-19
244 patients are transcriptionally active (Fig. 5e-g) in comparison to blood neutrophils (Extended
245 Data Fig. 5b) and further differentiate into a hyperinflammatory state (Fig. 5f). This is consistent
246 with more recent reports of neutrophil transmigration in other respiratory illnesses such as cystic
247 fibrosis[33], where neutrophils undergo lung/condition-specific adaptations upon recruitment from
248 the circulation[34] instead of the canonical rapid and transient effector function proceeding cell
249 death. Indeed, we observed increased expression of the interferon-stimulated gene (ISG) *IFI30*
250 along with increased expression of *CCL3* (MIP-1α) and *CCL4* (MIP-1β) (Fig. 5f), which in turn
251 can promote the recruitment of inflammatory monocytes to the lung and/or proinflammatory
252 macrophage phenotypes in the airways.
253
254 Importantly, most neutrophils increase expression of *CXCL8* (IL-8) when recruited to the
255 airways (Fig. 5d), perpetuating neutrophil recruitment to the lung. These findings further
256 corroborate our Hi-D flow cytometry, gene expression, and secreted protein data analysis
257 identifying IL-8 as the most abundant neutrophil-derived chemokine (and neutrophil chemotactic
258 factor) in the airways of severe COVID-19 patients. Furthermore, most neutrophils increase the
259 expression of *CXCR4* when recruited to the airways (Fig. 5f). Interestingly, we find that *CXCR4*
260 expression, previously attributed to immature neutrophils[16], is increased in mature lung-recruited
261 neutrophils (Fig. 5f). This is consistent with *CXCR4* expression dynamics previously detected in
262 non-COVID lung inflammation, including in cystic fibrosis[35] and malaria[36]. Taken together, the

263 progressive increase in *IFI30, CCL3/4*, along with abundant *de novo CXCL8* and *CXCR4* mRNA
264 transcripts, reveal a transcriptionally active state in neutrophils that is poised to sustain a
265 hyperinflammatory milieu in the lung of severe COVID-19 patients.
266
267 **Viral load in the respiratory tract does not correlate with disease severity**
268
269 We then investigated whether the recruited neutrophils or other cell types (i.e., myeloid,
270 lymphoid, and non-immune cells) in the airways of severe patients were infected with SARS-
271 CoV-2. By including the SARS-CoV-2 genome sequence into our human reference
272 transcriptome in the multi-omics single-cell analysis, we were able to assess viral mRNA
273 (vRNA) transcripts at a single-cell level (Fig. 7a). Notably, we did not detect vRNA in any cell
274 types in the blood or airways of severe patients (Fig. 7b,c). Further, SARS-CoV-2-specific RT-
275 qPCR revealed that viral load was decreased in the upper airways of severe patients admitted
276 to the ICU compared to mild-acute patients (Fig. 7d,e). However, we did note a gene signature
277 in neutrophils associated with response to IFN-γ (Fig. 5g and Extended Data Fig. 5b), including
278 a pronounced increase in *IFITM2* (Extended Data Fig. 5c), which has been shown to promote
279 SARS-CoV-2 infection in human lung cells[37].
280
281
282 **Pulmonary TNF and IL-1β promote neutrophil reprogramming in the lungs**
283
284 To ascertain which ligand-receptor pairs are potentially responsible for the transcriptional
285 reprogramming of neutrophils in the lung, we first performed differential gene expression (DGE)
286 analysis between blood neutrophil cluster 2 and lung neutrophils to identify genes that are
287 upregulated in lung-recruited neutrophils (Fig. 6a). Next, we used the computational method
288 NicheNet[38] to identify the potential (prioritized) ligands that could induce the upregulation of the
289 genes identified by the DGE analysis, indicating their potential role in neutrophil reprogramming
290 in the lung. *TNF*, *IL1B*, and *APOE* were the highest prioritized ligands with high ligand activity
291 whose signaling axes have the regulatory potential to drive gene expression profiles observed in
292 lung-recruited neutrophils (Fig. 6b). Importantly, NicheNet analysis revealed *TNF* as the ligand
293 predicted to increase *BCL2A1* expression in pulmonary neutrophils, as well as *CCL4* (MIP-1β)
294 and *CXCL16*. Furthermore, both *TNF* and *IL1B* are the ligands predicted to induce *NFKBIA* and
295 *CXCL8* (IL-8), and *IL1B* shows the greatest potential to induce *CCL3* (MIP-1α) expression in
296 recruited neutrophils. *APOE* is predicted to upregulate the expression of *FCER1G* in neutrophils
297 in the lung. Notably, *TNF, IL1B,* and *HMGB1* are the ligands that have the widest range of
298 regulatory potential, inducing neutrophil reprogramming by upregulating most genes that we
299 identified as differentially expressed (Fig. 6a) in lung-recruited neutrophils (Fig 6b).
300
301 Pulmonary T cells represent the primary cell population expressing *TNF* in the airways, where
302 MdCs have the highest *IL1B* and *APOE* transcripts (Fig. 6c,e). From the transcriptome data,
303 ligand-receptor pair analyses further identified putative signaling mediators for the top 15
304 prioritized ligands (Fig. 6d). *TNF* is predicted to signal through a receptor that has a *CALM1*
305 association (Fig. 6d). Intriguingly, it has been previously reported that CALM1 can bind other
306 transmembrane proteins, including ACE-2[39], and regulate their cell surface expression[40]. *IL1B* is
307 predicted to signal through the canonical IL1B/IL1R2 pathway, and *APOE* through the
308 APOE/SORL1 lipid pathway. *HMGB1* is predicted to signal through *LY96* (MD-2), which is
309 commonly associated with TLR4 (Fig. 6d)[41, 42, 43]. Accordingly, *IL1R2* and *CALM1* transcripts are

abundant in neutrophils from blood cluster 2, and their expression are sustained upon recruitment to the airways (Fig. 6e).

Collectively, we show here that TNF- and IL-1β-mediated transcriptional reprogramming of lung infiltrating neutrophils leads to induction of proinflammatory *NFKBIA*, *CCL3* (MIP-1α), and *CCL4* (MIP-1β) along with *TNFAIP3/6* and *CXCL8* (Figs. 5 and 6). Of note, neutrophil-derived *CCL3* and *CCL4* can attract inflammatory monocytes from the circulation to the airways. Interestingly, lung-infiltrating monocytes also produce elevated levels of *CXCL8*, potentiating the recruitment of circulating neutrophils via the CXCL8/CXCR2 axis (Fig. 5a,d). Hence, both neutrophils and inflammatory monocytes in the airways exacerbate and potentiate pathogenic neutrophilia in the lungs of severe patients in a positive feedback loop.

Discussion

Previous studies have reported increased neutrophilia in severe COVID-19, particularly in the circulation[14, 44, 45, 46]. In contrast, reports on exacerbated airway neutrophilia and the implication of lung neutrophils as the main cell type driving ARDS in severe patients have yielded inconclusive results[7, 8, 17, 47]. Here, we present the first comprehensive study of the lung immune response to SARS-CoV-2 in Black/AA individuals and unequivocally identify a robust and sustained airway neutrophilia associated with disease severity. The COVID-19 pandemic further highlighted some of the socio-economic and behavioral inequalities that may have contributed to troubling disparities in COVID-19-associated morbidity and mortality[48], with almost 70% of deaths being Black/AA patients in some areas[1, 2]. Although the socio-economic and behavioral differences indeed contribute to health disparities among demographics, a systematic investigation to determine the immunological features that characterize disease severity within Black/AA patients is lacking. Our systems biology approach addresses this knowledge gap and reveals new therapeutic targets to inhibit neutrophil migration, retention, and/or survival in the lung as potential effective interventions for individuals with severe disease that have been disproportionally affected by COVID-19.

Although previous studies on severe COVID-19 in humans have not been conclusive with regards to the role of airway neutrophilia in ARDS, studies in SARS-CoV-2-infected rhesus macaques and mice, where conditions and sample collection are more controlled, have identified exacerbated neutrophilia as a key immunological feature associated with disease severity[49, 50, 51]. Hence, taken together with previous studies on neutrophils[8, 14, 17, 45, 46, 47] along with animal models[49, 50, 51], our current findings provide compelling evidence that targeting exacerbated airway neutrophilia may constrain ARDS and prevent further lung damage in most patients requiring mechanical ventilator support. Although our studies represent one of the few targeted investigations in Black/AA patients, we believe our results have broader implications and may apply to most patients suffering from neutrophilic ARDS[11].

The heightened numbers of neutrophils in the lung are likely to induce and sustain inflammatory signatures by an autocrine/paracrine feedback loop among neutrophils, and paracrine signaling to other cell types that can potentiate disease severity. Notably, NE is a potent serine protease that we show is released from degranulating neutrophils in the lungs (see Fig. 2), and has potential to stimulate production of TNF, IL-1β, and IL-8[52, 53], and also abrogate protective effector functions of T cells and MdCs in the lung by cleaving cell surface receptors such as TLRs and Fc-receptors[54, 55]. Indeed, we demonstrate NE staining on the surface of T cells and MdCs in the lung (see Extended Data Fig. 5e) in addition to neutrophils, which may explain, in part, the reduction of FcγRII (CD32) expression on pulmonary neutrophils (see Extended Data Fig. 5a). Of note, the reduction in CD32 expression may prevent IgG-mediated suppression of ISG induction[14] in pulmonary neutrophils. Indeed, we demonstrate a pronounced signature for the ISG *IFI30* (see Fig. 5f). Similarly, we show by intracellular staining that pulmonary neutrophils are producing exacerbated levels of IL-1β protein that is likely released upon degranulation along with IL-8 and IL-6 (see Figs. 2 and 3). In addition to neutrophils, the myeloid lineage is also abundant in the airways and as such they are poised to influence disease

365 progression. For example, we and others[16] have shown that infiltrating neutrophils sustain local
366 production of calgranulins (S100A8/9/11/12), which can signal through and activate myeloid
367 cells via TLRs and RAGE receptors, compounding the already hyperinflammatory lung milieu.
368 Interestingly, the inflammatory monocytes that are likely recruited to the lungs via neutrophil-
369 secreted CCL3/4 also show elevated levels of neutrophil chemotactic factor *CXCL8* (IL-8),
370 which helps sustain recruitment of pathogenic neutrophils in a positive feedback loop.
371
372 Other immune and non-immune cell populations in the lung may contribute to COVID-19
373 pathogenesis in severe patients. Non-immune cells (e.g., stromal and epithelial cells) are known
374 targets of SARS-CoV-2 in the lung[56]. Therefore, these cells are also posited to influence
375 immune cell dynamics, especially at the outset of infection[57]. Indeed, our data indicate that non-
376 immune cells play a role in granulocyte activation (Extended Data Fig. 5d) and therefore may
377 initiate neutrophilia at the outset of infection[58]. Additionally, T cell-derived TNF and HMGB1,
378 along with myeloid-derived IL-1β, have regulatory potential to induce inflammatory gene
379 signatures observed in lung-recruited neutrophils. Strikingly, TNF is the ligand predicted to
380 increase *BCL2A1* expression in pulmonary neutrophils, which is an anti-apoptotic factor known
381 to regulate neutrophil survival[59, 60]. *TNF* signaling in recruited neutrophils also has the potential
382 to drive *CCL4* (MIP-1β) expression, along with *CXCL16*, which is another chemotactic factor
383 that can recruit neutrophils and macrophages via the CXCL16/CXCR6 pathway[61, 62]. In addition,
384 myeloid-derived *APOE* is predicted to regulate the expression of *FCER1G* in lung-recruited
385 neutrophils, which is associated with neutrophil activation during other viral respiratory
386 infections[63]. Further studies should investigate other effector functions of myeloid and lymphoid
387 subsets and how these cells interact with neutrophils to promote protection or pathology in the
388 lungs of severe COVID-19 patients.
389
390 Interestingly, *CXCR4* is upregulated in recruited neutrophils in severe patients (Figs. 4d,i and
391 5f), which may promote neutrophil survival and retention during pneumonitis and/or further
392 influence inflammatory neutrophil phenotype. Accordingly, CXCR4 was shown to promote
393 transcriptional reprogramming of neutrophils in pulmonary tissues[64]. Although we do not find
394 detectable levels of the canonical CXCR4 ligand (i.e., CXCL12) in the airways, we did observe
395 transcripts for *HMGB1* (Fig. 6), which is an alternative ligand for CXCR4. Since the IL-8/CXCR2
396 pathway is most notably increased and likely the primary neutrophil recruitment axis to the
397 airways, we speculate that CXCR4 signaling instead may promote neutrophil survival and
398 retention at the site of inflammation, which has been previously reported[65]. Additionally, CXCR4
399 signaling can stimulate de novo *CXCL8*/IL-8 production[66, 67], and has been shown to promote
400 neutrophil extracellular trap release during malaria disease progression[68]. Alternatively, CXCR4
401 is also associated with neutrophil aging and senescence[69, 70, 71]. As such, elevated CXCR4 may
402 be associated with prolonged neutrophil survival in COVID-19 pathogenesis. In a prior study[72],
403 we noted a similar pattern of CXCR4 expression on T cells from severe COVID-19 patients,
404 where a progressive decrease of surface CXCR4 is associated with recovery. In contrast,
405 patients that succumbed to the disease, showed a time-dependent escalation in $CXCR4^+$
406 circulating T cells concomitant to increased $CXCR4^+$ T cells in the lungs[72], implicating CXCR4
407 on the dysregulated lung-homing inflammatory T cells in COVID-19. Further investigation into
408 the potential role of CXCR4 in cell survival, retention, or recruitment may unravel novel

409 therapeutic targets to modulate inflammation and treat severe COVID-19. Notably, therapeutic
410 intervention with a CXCR4 antagonist during malaria-associated ARDS has shown significant
411 benefit in animal models[36].
412
413 Modulating inflammation through corticosteroids (particularly dexamethasone) has shown
414 clinical efficacy and is now the standard-of-care for patients progressing to severe COVID-19[73].
415 However, the pleiotropic effects of glucocorticoids and their propensity to cause neutrophilia are
416 well documented in asthma and chronic obstructive pulmonary disease (COPD)[74]. Although a
417 well-established mechanism of action for dexamethasone is via transcriptional repression of
418 proinflammatory cytokines, we observed very high *CXCL8* and *IL1B* transcripts concomitant
419 with elevated pulmonary IL-8 and IL-1β protein with prominent signatures by intracellular
420 staining—particularly in pulmonary neutrophils. In contrast, IL-6 levels were lower than that of
421 IL-8 and IL-1β in our patient cohort, and overly abundant neutrophils were not producing as
422 much IL-6 comparatively, which may explain, in part, why anti-IL-6/IL-6R studies failed to meet
423 primary endpoints[75]. Here, we provide evidence of an uncoupled cytokine profile in airway fluids
424 versus plasma where the lung microenvironment exhibits features of cytokine-induced ARDS
425 driven largely by a proinflammatory, neutrophilic feed-forward loop. Beyond COVID-19, it has
426 been shown that resolution of neutrophilia in ARDS has substantial prognostic benefit[10]. Taken
427 together, the CXCL8 (IL-8)/CXCR2 signaling axis emerges as a key potential target for next-
428 generation immunomodulatory therapy to reduce pathogenic neutrophilia and constrain severe
429 disease in patients in addition to corticosteroids.
430
431 We also contend that recognizing the lung pathology in severe COVID-19 to be a neutrophilic
432 and hyperinflammatory disease is paramount to achieve better outcomes in next-generation
433 therapies. Although the lung pathology in COVID-19 is initiated by a viral infection, severe
434 patients in the ICU no longer show signs of uncontrolled viral replication. In fact, not only did we
435 not detect viral transcripts by scRNA-seq within the cells in the airways, but we also noted
436 decreased viral burden in severe patients in the ICU versus mild-acute patients seen in the
437 outpatient clinic (Fig. 7). This is further supported by our previous study where we performed
438 plaque assays on the respiratory secretions from severe patients and revealed significantly
439 diminished, if any, viral plaques from the endotracheal aspirates[76]. This may explain, in part,
440 why antiviral drugs such as remdesivir are not able to prevent death when administered to
441 severe patients in ICU[77].
442
443 It is important to consider potentially confounding factors and limitations in our study. Though a
444 major strength of our study is the uniformity of sample collection in a single disease state, our
445 airway samples are limited to ETA, which contrasts with bronchoalveolar lavage fluid (BALF)
446 used in other studies[7, 17]. The ETA procedure can sample material from the medial airways—
447 i.e., an intermediate between the distal/lower airways (e.g., BALF) and the proximal/upper
448 airways (e.g., sputum or oro-/naso-pharyngeal samples). Although the relative abundance of
449 immune cells may vary across the upper and lower airways, previous studies observe a
450 correlation between paired ETA and BALF samples. In addition, these studies show that ETA
451 samples are not inherently neutrophilic[78], though neutrophilia/granulocytosis may be a shared
452 feature of non-COVID-19 and COVID-19 ARDS[10, 79]. In any event, our study is one of the only

453 known to date to employ integrated multi-omics single-cell investigation of immunity in
454 exclusively Black/AA subjects, which are disproportionately burdened with severe disease and
455 worse outcomes. Importantly, other studies of COVID-19 immune responses have noted similar
456 features of disease severity[7, 15, 16], which suggests that the findings in our target demographic
457 will be broadly applicable to other groups. Finally, our study was limited in scope to 35 total
458 subjects and single collection time points, limiting our abilities to interrogate correlations with
459 clinical outcomes, warranting further longitudinal studies in larger patient cohorts.
460
461 In conclusion, we present evidence that neutrophils are poised to be the leukocyte population
462 most responsible for the dysregulated hyperinflammatory response that drives ARDS in severe
463 COVID-19 patients. Neutrophil frequency and inflammatory profiles reveal that they are not only
464 the most abundant leukocyte population in the medial airways, but also major producers of
465 hallmark effector molecules associated with disease severity, including IL-8, IL-1β, and IL-6,
466 along with potent proteases such as NE and MPO, which are inherently inflammatory and
467 contribute to lung damage/pathology. Furthermore, we provide evidence for a neutrophil
468 feedforward loop where IL-8, produced by virtually all pulmonary neutrophils (and some myeloid
469 and stromal cells), is the primary chemokine recruiting circulating neutrophils and promoting
470 neutrophilia in the inflamed airways.
471
472 Collectively, our findings implicate neutrophilia in the immunopathophysiology of severe COVID-
473 19 disease where perpetual, transcriptionally active, and highly inflammatory pulmonary
474 neutrophils drive ARDS despite low viral burden. Thus, therapeutic intervention targeting
475 neutrophil recruitment/retention and/or survival/reprogramming at the site of inflammation has
476 the potential to constrain ARDS in severe patients, particularly those most vulnerable to
477 succumb to COVID-19 disease.

Methods

Ethics and biosafety. A total of 35 individuals were recruited for this study (Extended Data Tables 1 and 2). The 18 severe COVID-19+ patients were recruited from the Intensive Care Units of Emory University, Emory St. Joseph's, Emory Decatur, and Emory Midtown Hospitals. We also recruited 9 mild COVID-19-infected outpatients in the Emory Acute Respiratory Clinic and 8 healthy adults from the Emory University Hospital. All studies were approved by the Emory Institutional Review Board (IRB) under protocol numbers IRB00058507, IRB00057983, and IRB00058271. Informed consent was obtained from the patients when they had decision-making ability or from a legally authorized representative (LAR) if the patient was unable to provide consent. Blood and sputum or endotracheal aspirate (ETA) were obtained. Control blood samples were obtained from healthy adults matched by age and race. Study inclusion criteria included a confirmed COVID-19 diagnosis by PCR amplification of SARS-CoV-2 viral RNA obtained from nasopharyngeal or oropharyngeal swabs, age of 18 years or greater, and willingness to provide informed consent. Individuals with a confirmed history of COVID-19 diagnosis were excluded from the healthy donor group. All work with infectious virus and respiratory samples from COVID-19 patients was conducted inside a biosafety cabinet within the Emory Health and Safety Office (EHSO) and the United States Department of Agriculture (USDA)-approved BSL3 containment facility in the Health Sciences Research Building at Emory University following protocols approved by the Institutional Biosafety Committee (IBC) and Biosafety Officer (see ref[76]).

Patient sample collection and processing. Primary leukocytes from the airways of COVID-19 patients requiring mechanical ventilator support were collected bedside via endotracheal aspiration (ETA) and whole blood collected by standard venipuncture. Plasma from whole blood was isolated via centrifugation at 400 x g for 10 min at 4˚C. To remove platelets, the isolated plasma was centrifuged at 4,000 x g for 10 min at 4˚C. Untouched circulating leukocytes were isolated using the EasySep™ RBC Depletion Reagent (StemCell Technologies). ETA (from severe patients) or non-induced sputum (from mild patients) was mixed 1:1 with a 50mM EDTA solution (final concentration 25 mM EDTA) in custom RPMI-1640 media deficient in biotin, L-glutamine, phenol red, riboflavin, and sodium bicarbonate (defRPMI-1640), with 3% newborn calf serum (NBCS) and mechanically dissociated using a syringe to liberate leukocytes from mucins and other respiratory secretions. Supernatants were collected for further analysis, and then cells underwent an additional mechanical dissociation step using 1-3 mL of a 10 mM EDTA in defRPMI-1640 + 3% NBCS and a P1000 pipettor. Cells were then washed with 10 mL defRPMI-1640 + 3% NBCS, passed through a 70 µm nylon strainer, and pelleted through a 2 mL 100% NBCS layer prior to counting and downstream processing.

High-dimensional (Hi-D) 30-parameter flow cytometry. Cells (up to 10^7 total) were resuspended in defRPMI-1640 with 3% newborn calf serum and Benzonase™ (FACS buffer) in 5 mL FACS tubes and pre-incubated with GolgiStop™ (BD Biosciences) for ~60 min at 4˚C. Human TruStain FcX™ was then added, followed by a 10 min incubation at RT. The 24-color extracellular staining master mix (Extended Data Table 2) was prepared 2X in BD Horizon™ Brilliant Stain Buffer to prevent staining artifacts from BD Horizon Brilliant dye interactions and

522 added 1:1 to cells, then incubated for 30 min at 4˚C. Following staining (and total 1 h exposure
523 to GolgiStop™), cells were washed with ~4 mL FACS buffer. Next, the cells were resuspended
524 in 200 µL of BD Cytofix/Cytoperm™ fixation/permeabilization solution and incubated at 4˚C for
525 30 min followed by a wash with ~4 mL BD Perm/Wash™ Buffer. The 4-color intracellular
526 staining (Extended Data Table 3) was prepared in BD Perm/Wash™ Buffer, and cells were
527 stained for 30 min at 4˚C. Cells were washed with ~4 mL BD Perm/Wash™ Buffer, then
528 resuspended for a final 20 min incubation in 4% PFA and transported out of the BSL3
529 containment facility. Cells were washed in ~4 mL FACS buffer, then resuspended in 200-1000
530 µL FACS buffer for acquisition using BD FACSDiva™ Software on the Emory Pediatric/Winship
531 Flow Cytometry Core BD FACSymphony™ A5. To distinguish auto-fluorescent cells from cells
532 expressing low levels of a particular surface marker, we established upper thresholds for auto-
533 fluorescence by staining samples with fluorescence-minus-one (FMO) control stain sets in
534 which a reagent for a channel of interest is omitted. Data were analyzed with FlowJo™ v10.8
535 (FlowJo LLC).
536
537 **Cell-surface antibody-derived tag (ADT) staining, single-cell encapsulation, and library**
538 **generation.** Leukocytes from whole blood and ETA samples were incubated with oligo-
539 conjugated Ig-A/D/G/M for 10 min at 4˚C followed by the addition of Human TruStain FcX™
540 (BioLegend) and 10 min incubation at RT. Cells were then surface stained with oligo-conjugated
541 monoclonal antibody panel (total 89 antibodies; Extended Data Table 5) for 30 min at 4˚C,
542 followed by two washes in def-RPMI-1640/0.04% BSA. Cells were resuspended at a
543 concentration of 1200-1500 cells/µL in def-RPMI-1640/0.04% BSA and passed through a 20 or
544 40 µm cell strainer before loading onto a Chromium Controller (10X Genomics, Pleasanton,
545 CA). Cells were loaded to target encapsulation of 10,000 cells. Gene expression (GEX) and
546 antibody-derived tag (ADT) libraries were generated using the Chromium Single Cell 5′ Library
547 & Gel Bead Kit v1.1 with feature barcoding following the manufacturer's instructions. GEX
548 libraries were pooled and sequenced at a depth of approximately 540,000,000 reads per sample
549 in a single S4 flow cell and ADT libraries at a depth of approximately 79,000,000 reads per
550 sample in a single lane of an S4 flow cell on a NovaSeq™ 6000 (Illumina, San Diego, CA;
551 Extended Data Table 6)
552
553 **Multi-omics single-cell RNA sequencing (scRNA-seq) analysis.** Single-cell 5′ unique
554 molecular identifier (UMI) counting and barcode de-multiplexing were performed using
555 CellRanger Software (v.5.0.0). To detect SARS-CoV-2 viral RNA reads, we built a custom
556 reference genome from human GRCh38 and SARS-CoV-2 references (severe acute respiratory
557 syndrome coronavirus 2 isolate Wuhan-Hu-1, complete genome, GenBank MN908947.3).
558 Splicing-aware aligner STAR[80] was implemented to align FASTQ inputs to the reference
559 genome, and the resulting files are automatically filtered by CellRanger to include only cell
560 barcodes representing real cells. This determination is based on the distribution of UMI counts.
561 ADT reads were aligned to a feature reference file containing the antibody-specific barcode
562 sequences. To recover neutrophils, we applied our SuPERR-seq pipeline as previously
563 described[30]. Briefly, we recovered neutrophils from CellRanger unfiltered count matrices by
564 plotting surface CD16 ADT and CD66b ADT using the "FeatureScatter" function in Seurat v4.0[81]
565 (R version 4.0.2). The double-positive cell barcodes were then extracted and further evaluated

566 by GEX to confirm viable neutrophil identity. A threshold for mitochondrial content per barcode
567 was determined for each sample independently and applied as a cutoff to remove dead or dying
568 cells (Extended Data Table 7). Most samples show high cell viability with a minimal proportion of
569 dead cells.
570
571 The UMI counts of the GEX data were log-normalized by the "NormalizeData" function in Seurat
572 before downstream analysis, following the optimal workflow we previously described for sample
573 normalization and data integration[82]. Center log-ratio (CLR) transform in Seurat was performed
574 on ADT UMIs when recovering neutrophils from the unfiltered matrices. For surface protein
575 visualization to classify major lineages using our SuPERR-seq workflow[30], ADT UMIs were
576 normalized using the R package Denoised and Scaled by Background[83] (DSB) to remove
577 ambient UMI counts (i.e., background) prior to manual sequential gating by surface expression
578 (Extended Data Fig. 4) in SeqGeq v1.7 (FlowJo, LLC). DSB uses empty droplets to calculate
579 background expression, which was manually selected according to the distribution of total ADT
580 per cell in the raw count matrices (Extended Data Table 8). To minimize the influence from non-
581 informative empty droplets, we removed cell barcodes with less than 100 total ADT UMIs before
582 plotting the ADT distribution.
583
584 Before integrating the multiple datasets, we first classified major lineages in individual samples
585 based on a combination of gene transcript and surface protein markers (SuPERR-seq
586 workflow[30]) as in Fig. 4 for samples where the ADT library was of sufficient quality to allow
587 manual gating (Extended Data Fig. 4). Cell barcodes within each major lineage that co-
588 expressed markers exclusive to other major lineages were considered cell doublets and
589 removed (Extended Data Fig. 4). In addition, we removed cell barcodes with extremely high
590 total ADT UMIs, which we considered to be aggregated cells. To efficiently integrate replicate
591 samples, we concatenated major lineages derived from the same tissue in different donors. To
592 minimize batch effects and optimize data integration, we followed the data normalization and
593 merging strategies described previously[82]. Briefly, samples were first treated individually, and
594 log-normalized count matrices were scaled/Z-transformed, and the "vst" method of the Seurat
595 function "FindVariableFeatures" was utilized to select the top 1000 highly variable genes
596 (HVGs) of each sample. HVGs shared between replicate samples were used to perform
597 principal component analysis (PCA). To visualize the data, we performed UMAP reduction of
598 the first 30 PCs, and cell clustering was generated using the Leiden community detection
599 algorithm at a resolution of 0.8. UMAP visualizations for the integrated Blood and integrated
600 ETA were generated using Seurat v4 data integration workflow.
601
602 **Receptor-ligand interaction analyses**. Clustered cells from lung and blood samples from each
603 patient were investigated for evidence of intercellular communication using CellChat[31].
604 Clustered cell populations from the lung samples were combined with the blood neutrophils to
605 determine which lung cell populations could recruit circulating neutrophils. We utilized
606 NicheNet[38] to determine which ligand-receptor pairs could be responsible for the different
607 transcriptional states of the neutrophil populations in the lung and blood samples. We focused
608 on certain neutrophil clusters as the receiver populations, considering the remaining neutrophils
609 and other lung cell populations as the senders and thus potential interactors. The target set of

genes was determined using Seurat::FindMarkers(min.pct = 0.1), keeping only those genes with an adjusted p-value lower than 0.05 and average log2-fold change of more than 0.2. To address gene expression changes due to lung infiltration, we ran the algorithm using blood neutrophil cluster 2 as the most likely candidate for lung infiltration. The genes considered were those differentially expressed between blood cluster 2 and the lung neutrophils and genes differentially expressed between blood cluster 2 and those cells that progress along "Trajectory 2" in the lung (see Fig.5).

Cell trajectory analyses. The Python toolkit scVelo[32] inferred the trajectories using biological data of the ETA neutrophils. Input data for scVelo analysis was intron, exon, and spanning count matrices estimated using the dropEST tool[84], then filtered with previously identified neutrophil cell barcodes in R studio. Intron, exon, and spanning matrices were compared to identify missing rows (genes) and were added to each matrix to equalize dimensions. The exon matrix contained the spliced matrix, and the sum of the intron and spanning matrices constituted the unspliced matrix. Spliced and unspliced matrices were imported with anndata library, and pandas library was used to import gene names and cell barcodes. Raw count matrices were added to anndata object layers as 'spliced' and 'unspliced.' Then, gene names and cell barcodes were attached to variables and observations of anndata object, respectively. Anndata object was transposed, followed by the regular scVelo analysis. The default parameters of plotting velocity streams include vkey='velocity', colorbar=True, alpha=0.3, sort_order=True, and legend_loc='on data'.

Pathway and process enrichment analyses. Differential gene expression (DGE) analyses were performed in Seurat v4 and imported for gene annotation and further analysis using Metascape[85]. DGE between neutrophils versus the total ETA were used to generate Fig. 5g and non-immune cells versus total ETA were used for Extended Data Fig. 5d.

Mesoscale U-PLEX assays. U-PLEX Biomarker Group 1 Human Multiplex Assays (Meso Scale Discovery) were used to evaluate levels of 21 analytes following the manufacturer's protocol (Extended Data Table 4) in plasma and UVC-inactivated respiratory supernatants (see ref[76]). Samples were diluted 1:5 for all assays except for IL-8, MCP-1, and IL-1RA, which were above the upper limit of detection for the assay and were diluted 1:200 to acquire measurement within the assay range. Final values were obtained by multiplying measurements by their respective dilution factor.

Myeloperoxidase (MPO) content and activity. The abundance and activity of MPO were quantified as previously described[29]. MPO activity and protein concentration were measured sequentially following the immunocapture. On average, across six 96-well plate assays, lower limits of quantification were 4.0 ng/mL (activity) and 0.84 ng/mL (protein). Samples above the lower limit of detection but below the lower limit of quantification were imputed as half of the latter, and those detected above the highest standard of 50 ng/mL (i.e., above the upper limit of detection) at all dilutions were imputed as twice the standard concentration (Extended Data Table 4).

654 **SARS-CoV-2 quantitative reverse transcription PCR (RT-qPCR).** Viral (v)RNA was
655 extracted from the respiratory secretions of COVID-19 patients using the *Quick*-RNA™ Viral Kit
656 (Zymo Research) following the manufacturer's protocol and complementary (c)DNA synthesized
657 using the High-Capacity cDNA Reverse Transcription Kit (Applied Biosystems™) per the
658 manufacturer's instructions, then diluted 1:5 in nuclease-free water. 10 µL diluted cDNA was
659 used with the NEB Luna® Universal Probe qPCR Master Mix (New England BioLabs® Inc.)
660 following the manufacturer's protocol and performed in 384-well plates using a QuantStudio™ 5
661 Real-Time PCR System (Applied Biosystems™). Primer/probe pairs were:
662 AGAAGATTGGTTAGATGATGATAGT (forward), TTCCATCTCTAATTGAGGTTGAACC
663 (reverse), and /56-FAM/TCCTCACTGCCGTCTTGTTGACCA/3IABkFQ/ (probe), which were
664 designed from sequences previously described[86] (Integrated DNA Technologies; IDT). To
665 generate a standard curve for the quantification of SARS-CoV-2 genome copies a gBlock from
666 IDT with the following sequence was used as a standard:
667 AATTAAGAACACGTCACCGCAAGAAGAAGATTGGTTAGATGATGATAGTCAACAAACTGTT
668 GGTCAACAAGACGGCAGTGAGGACAATCAGACAACTACTATTCAAACAATTGTTGAGGTTC
669 AACCTCAATTAGAGATGGAACTTACAGTTTCAGTGTTCAATTAA.
670
671 **Statistical analyses**. Statistical analyses were performed using GraphPad Prism9. Data were
672 analyzed for distribution (normal (Gaussian) vs. lognormal) independently using the D'Agostino
673 and Pearson test for normality in the untransformed and Log10-transformed data. In cases
674 where the sample size (*N*) was too small for D'Agostino and Pearson normality test, the
675 Shapiro-Wilk test was used to assess distribution. When data passed both distribution tests, the
676 likelihood of each distribution (normal vs. lognormal) was computed, and QQ-plots were
677 generated. When Log10 transformed data had a higher likelihood of a normal distribution
678 (passing normal distribution test) and/or failed lognormal distribution test, paired t-tests were
679 performed to compare matching blood and respiratory supernatant samples within a single
680 group. If the data had unequal variance (as determined by an F-test), a ratio paired t-test was
681 performed. All instances where lognormal distribution was likely non-parametric Wilcoxon
682 matched-pairs sign ranked tests were performed. For comparisons across the three patient
683 groups (i.e., healthy, mild-acute, severe), ordinary one-way ANOVA (if equal variance) or
684 Brown-Forsythe and Welch ANOVA (if unequal variance) tests were performed for data with a
685 normal distribution. Alternatively, data with a lognormal distribution were analyzed with a
686 Kruskal-Wallis test.
687
688 **Data availability.** Single-cell sequencing datasets presented here are available through NCBI
689 GEO, accession number XXX.

Author Contributions

Devon J. Eddins: Conceptualization, Methodology, Investigation, Formal Analysis, Data Curation, Writing–Original Draft, Writing–Review & Editing, Visualization. **Junkai Yang**: Methodology, Formal Analysis, Data Curation, Writing–Review & Editing, Visualization. **Astrid Kosters**: Methodology, Investigation, Data Curation, Writing–Review & Editing. **Vincent D. Giacalone**: Methodology, Formal Analysis, Investigation, Data Curation, Writing–Review & Editing. **Ximo Pechuan**: Methodology, Formal Analysis, Data Curation, Visualization, Writing–Review & Editing. **Joshua D. Chandler**: Methodology, Formal Analysis, Investigation, Data Curation, Writing–Review & Editing. **Jinyoung Eum**: Formal Analysis, Visualization. **Benjamin R. Babcock**: Investigation, Data curation. **Brian S. Dobosh**: Investigation, Data Curation, Formal Analysis. **Mindy R. Hernández**: Resources. **Fathma Abdulkhader**: Investigation. **Genoah L. Collins**: Investigation. **Richard P. Ramonell**: Resources, Data Curation, Writing–Review & Editing. **Christine Moussion**: Methodology, Formal Analysis. **Darya Y. Orlova**: Methodology, Data Curation. **Ignacio Sanz**: Resources. **F. Eun-Hyung Lee**: Methodology, Data Curation, Resources, Writing–Review & Editing. **Rabindra M. Tirouvanziam**: Methodology, Formal Analysis, Data Curation, Resources, Writing–Review & Editing. **Eliver E.B. Ghosn**: Conceptualization, Methodology, Formal Analysis, Resources, Data Curation, Writing–Original Draft, Visualization, Supervision, Project Administration**,** Funding Acquisition**.** All authors discussed the results and read and approved the final manuscript.

Competing interests

FEL is the founder of MicroB-plex, Inc., serves on the SAB of Be Bio Pharma, receives grants from BMGF and Genentech, and receives royalties from BLI, inc. All other authors have no competing interest to declare.

Acknowledgments

This study was funded by NIH/NIAID R01AI123126 (EEBG) and R01AI123126-05S1 (EEBG), the Program for Breakthrough Biomedical Research (EEBG), and the Lowance Center for Human Immunology (EEBG). DJE was partially supported by the Emory's Laney Graduate School Fellowship, and RPR was supported by the NIH T32-HL116271-07 Fellowship. The graphical abstract and Fig. 7d were generated in part using BioRender. We thank Keivan Zandi, Ann Chahroudi, Nils Schoof, Kira Moresco, and Stacy Heilman of the Department of Pediatrics (Emory University) along with the Emory Biosafety Officers Kalpana Rengarajan and Esmeralda Meyer for their assistance with setting up the BLS3 facility and kindly providing SARS-CoV-2 viral stocks. We thank Nadia Roan (Gladstone Institutes/UCSF) and Sulggi Lee (UCSF) for helpful discussions. Flow cytometry data were collected at the Emory's Pediatrics/Winship Flow Cytometry Core (access supported in part by Children's Healthcare of Atlanta). We acknowledge the Genomic Cores at Yerkes Non-Human Primate Research Center at Emory University (NIH P51 OD011132; NIH S10 OD026799), Baylor College of Medicine, and the Parker H. Petit Institute for Bioengineering and Bioscience at the Georgia Institute of Technology for the single-cell library sequences. We are grateful for the efforts of Sang N. Le, John Varghese, Anum Jalal, Saeyun Lee, and Rahul Patel, who also contributed to patient recruitment. We also thank the nurses, staff, and providers in the 71 ICU in Emory University Hospital Midtown, the medical ICU in Emory Decatur Hospital, the 5G/6G ICU in Emory University Hospital, and the ICU in Emory Saint Joseph's Hospital for their dedication and commitment during the COVID-19 pandemic. We thank all healthy individuals, patients, and their families for their participation in this study, without whom our work would not have been possible.

References

1. Van Dyke, M.E. *et al.* Racial and ethnic disparities in COVID-19 incidence by age, sex, and period among persons aged< 25 years—16 US jurisdictions, January 1–December 31, 2020. *Morbidity and Mortality Weekly Report* **70**, 382 (2021).

2. Romano, S.D. *et al.* Trends in Racial and Ethnic Disparities in COVID-19 Hospitalizations, by Region - United States, March-December 2020. *MMWR Morb Mortal Wkly Rep* **70**, 560-565 (2021).

3. Lucas, C. *et al.* Longitudinal analyses reveal immunological misfiring in severe COVID-19. *Nature* **584**, 463-469 (2020).

4. Merad, M. & Martin, J.C. Pathological inflammation in patients with COVID-19: a key role for monocytes and macrophages. *Nature Reviews Immunology* **20**, 355-362 (2020).

5. Olwal, C.O. *et al.* Parallels in Sepsis and COVID-19 Conditions: Implications for Managing Severe COVID-19 Patients. *Frontiers in immunology* **12**, 91 (2021).

6. Carvalho, T., Krammer, F. & Iwasaki, A. The first 12 months of COVID-19: a timeline of immunological insights. *Nat Rev Immunol* **21**, 245-256 (2021).

7. Bost, P. *et al.* Deciphering the state of immune silence in fatal COVID-19 patients. *Nat Commun* **12**, 1428 (2021).

8. Liao, M. *et al.* Single-cell landscape of bronchoalveolar immune cells in patients with COVID-19. *Nat Med* **26**, 842-844 (2020).

9. Liang, W. *et al.* Development and Validation of a Clinical Risk Score to Predict the Occurrence of Critical Illness in Hospitalized Patients With COVID-19. *JAMA Intern Med* **180**, 1081-1089 (2020).

10. Steinberg, K.P. *et al.* Evolution of bronchoalveolar cell populations in the adult respiratory distress syndrome. *Am J Respir Crit Care Med* **150**, 113-122 (1994).

11. Barnes, B.J. *et al.* Targeting potential drivers of COVID-19: Neutrophil extracellular traps. *J Exp Med* **217** (2020).

12. Kong, M., Zhang, H., Cao, X., Mao, X. & Lu, Z. Higher level of neutrophil-to-lymphocyte is associated with severe COVID-19. *Epidemiology & Infection* **148** (2020).

13. Liu, Y. *et al.* Neutrophil-to-lymphocyte ratio as an independent risk factor for mortality in hospitalized patients with COVID-19. *Journal of Infection* (2020).

14. Combes, A.J. *et al.* Global absence and targeting of protective immune states in severe COVID-19. *Nature* **591**, 124-130 (2021).

15. Schulte-Schrepping, J. *et al.* Severe COVID-19 is marked by a dysregulated myeloid cell compartment. *Cell* **182**, 1419-1440 (2020).

16. Silvin, A. *et al.* Elevated Calprotectin and Abnormal Myeloid Cell Subsets Discriminate Severe from Mild COVID-19. *Cell* **182**, 1401-1418 e1418 (2020).

17. Grant, R.A. *et al.* Circuits between infected macrophages and T cells in SARS-CoV-2 pneumonia. *Nature* **590**, 635-641 (2021).

18. Wilk, A.J. *et al.* A single-cell atlas of the peripheral immune response in patients with severe COVID-19. *Nat Med* **26**, 1070-1076 (2020).

19. Kreutmair, S. *et al.* Distinct immunological signatures discriminate severe COVID-19 from non-SARS-CoV-2-driven critical pneumonia. *Immunity* **54**, 1578-1593 e1575 (2021).

20. Ren, X. *et al.* COVID-19 immune features revealed by a large-scale single-cell transcriptome atlas. *Cell* **184**, 1895-1913 e1819 (2021).

21. Xu, G. *et al.* The differential immune responses to COVID-19 in peripheral and lung revealed by single-cell RNA sequencing. *Cell Discov* **6**, 73 (2020).

22. Forrest, O.A. *et al.* Frontline Science: Pathological conditioning of human neutrophils recruited to the airway milieu in cystic fibrosis. *J Leukoc Biol* **104**, 665-675 (2018).

23. Szabo, P.A. *et al.* Longitudinal profiling of respiratory and systemic immune responses reveals myeloid cell-driven lung inflammation in severe COVID-19. *Immunity* **54**, 797-814 (2021).

24. Jouan, Y., Baranek, T., Si-Tahar, M., Paget, C. & Guillon, A. Lung compartmentalization of inflammatory biomarkers in COVID-19-related ARDS. *Critical Care* **25**, 1-3 (2021).

25. Zaid, Y. *et al.* Chemokines and Eicosanoids Fuel the Hyperinflammation Within the Lungs of Patients with Severe COVID-19. *Journal of Allergy and Clinical Immunology* (2021).

26. Jouan, Y. *et al.* Phenotypical and functional alteration of unconventional T cells in severe COVID-19 patients. *J Exp Med* **217** (2020).

27. Satış, H. *et al.* Prognostic value of interleukin-18 and its association with other inflammatory markers and disease severity in COVID-19. *Cytokine* **137**, 155302 (2021).

28. Yang, Y. *et al.* Plasma IP-10 and MCP-3 levels are highly associated with disease severity and predict the progression of COVID-19. *Journal of Allergy and Clinical Immunology* **146**, 119-127 (2020).

29. Chandler, J.D. *et al.* Myeloperoxidase oxidation of methionine associates with early cystic fibrosis lung disease. *Eur Respir J* **52** (2018).

30. Xu, C. *et al.* Comprehensive multi-omics single-cell data integration reveals greater heterogeneity in the human immune system. *bioRxiv*, 2021.2007.2025.453651 (2021).

31. Jin, S. *et al.* Inference and analysis of cell-cell communication using CellChat. *Nature communications* **12**, 1-20 (2021).

842 32. Bergen, V., Lange, M., Peidli, S., Wolf, F.A. & Theis, F.J. Generalizing RNA velocity to
843 transient cell states through dynamical modeling. *Nat Biotechnol* **38**, 1408-1414 (2020).
844
845 33. Margaroli, C. *et al.* Transcriptional firing represses bactericidal activity in cystic fibrosis
846 airway neutrophils. *Cell Rep Med* **2**, 100239 (2021).
847
848 34. Giacalone, V.D., Margaroli, C., Mall, M.A. & Tirouvanziam, R. Neutrophil Adaptations
849 upon Recruitment to the Lung: New Concepts and Implications for Homeostasis and
850 Disease. *International Journal of Molecular Sciences* **21**, 851 (2020).
851
852 35. Makam, M. *et al.* Activation of critical, host-induced, metabolic and stress pathways
853 marks neutrophil entry into cystic fibrosis lungs. *Proc Natl Acad Sci U S A* **106**, 5779-
854 5783 (2009).
855
856 36. Sercundes, M.K. *et al.* Targeting Neutrophils to Prevent Malaria-Associated Acute Lung
857 Injury/Acute Respiratory Distress Syndrome in Mice. *PLoS Pathog* **12**, e1006054 (2016).
858
859 37. Prelli Bozzo, C. *et al.* IFITM proteins promote SARS-CoV-2 infection and are targets for
860 virus inhibition in vitro. *Nature Communications* **12**, 1-13 (2021).
861
862 38. Browaeys, R., Saelens, W. & Saeys, Y. NicheNet: modeling intercellular communication
863 by linking ligands to target genes. *Nat Methods* **17**, 159-162 (2020).
864
865 39. Chattopadhyay, S. *et al.* Calmodulin binds to the cytoplasmic domain of angiotensin-
866 converting enzyme and regulates its phosphorylation and cleavage secretion. *J Biol*
867 *Chem* **280**, 33847-33855 (2005).
868
869 40. Lambert, D.W., Clarke, N.E., Hooper, N.M. & Turner, A.J. Calmodulin interacts with
870 angiotensin-converting enzyme-2 (ACE2) and inhibits shedding of its ectodomain. *FEBS*
871 *letters* **582**, 385-390 (2008).
872
873 41. Shimazu, R. *et al.* MD-2, a molecule that confers lipopolysaccharide responsiveness on
874 Toll-like receptor 4. *J Exp Med* **189**, 1777-1782 (1999).
875
876 42. Visintin, A., Mazzoni, A., Spitzer, J.A. & Segal, D.M. Secreted MD-2 is a large polymeric
877 protein that efficiently confers lipopolysaccharide sensitivity to Toll-like receptor 4. *Proc*
878 *Natl Acad Sci U S A* **98**, 12156-12161 (2001).
879
880 43. Yang, H. *et al.* A critical cysteine is required for HMGB1 binding to Toll-like receptor 4
881 and activation of macrophage cytokine release. *Proc Natl Acad Sci U S A* **107**, 11942-
882 11947 (2010).
883
884 44. Bohn, M.K. *et al.* Pathophysiology of COVID-19: Mechanisms Underlying Disease
885 Severity and Progression. *Physiology (Bethesda)* **35**, 288-301 (2020).
886
887 45. Meizlish, M.L. *et al.* A neutrophil activation signature predicts critical illness and mortality
888 in COVID-19. *Blood Adv* **5**, 1164-1177 (2021).
889
890 46. Metzemaekers, M. *et al.* Kinetics of peripheral blood neutrophils in severe coronavirus
891 disease 2019. *Clin Transl Immunology* **10**, e1271 (2021).
892

47. Wauters, E. *et al.* Discriminating mild from critical COVID-19 by innate and adaptive immune single-cell profiling of bronchoalveolar lavages. *Cell Res* **31**, 272-290 (2021).

48. Abedi, V. *et al.* Racial, economic, and health inequality and COVID-19 infection in the United States. *Journal of racial and ethnic health disparities* **8**, 732-742 (2021).

49. Guo, Q. *et al.* Induction of alarmin S100A8/A9 mediates activation of aberrant neutrophils in the pathogenesis of COVID-19. *Cell Host Microbe* **29**, 222-235 e224 (2021).

50. Hoang, T.N. *et al.* Baricitinib treatment resolves lower-airway macrophage inflammation and neutrophil recruitment in SARS-CoV-2-infected rhesus macaques. *Cell* **184**, 460-475 e421 (2021).

51. Vanderheiden, A. *et al.* CCR2-dependent monocyte-derived cells restrict SARS-CoV-2 infection. *bioRxiv* (2021).

52. Krotova, K., Khodayari, N., Oshins, R., Aslanidi, G. & Brantly, M.L. Neutrophil elastase promotes macrophage cell adhesion and cytokine production through the integrin-Src kinases pathway. *Sci Rep* **10**, 15874 (2020).

53. Towstyka, N.Y. *et al.* Modulation of γδ T-cell activation by neutrophil elastase. *Immunology* **153**, 225-237 (2018).

54. Domon, H. *et al.* Neutrophil Elastase Subverts the Immune Response by Cleaving Toll-Like Receptors and Cytokines in Pneumococcal Pneumonia. *Front Immunol* **9**, 732 (2018).

55. Kim, E. *et al.* Inhibition of elastase enhances the adjuvanticity of alum and promotes anti-SARS-CoV-2 systemic and mucosal immunity. *Proc Natl Acad Sci U S A* **118** (2021).

56. Delorey, T.M. *et al.* COVID-19 tissue atlases reveal SARS-CoV-2 pathology and cellular targets. *Nature* **595**, 107-113 (2021).

57. Chua, R.L. *et al.* COVID-19 severity correlates with airway epithelium-immune cell interactions identified by single-cell analysis. *Nat Biotechnol* **38**, 970-979 (2020).

58. Qi, F. *et al.* ScRNA-seq revealed the kinetic of nasopharyngeal immune responses in asymptomatic COVID-19 carriers. *Cell Discov* **7**, 56 (2021).

59. Jenal, M. *et al.* The anti-apoptotic gene BCL2A1 is a novel transcriptional target of PU.1. *Leukemia* **24**, 1073-1076 (2010).

60. Vier, J., Groth, M., Sochalska, M. & Kirschnek, S. The anti-apoptotic Bcl-2 family protein A1/Bfl-1 regulates neutrophil survival and homeostasis and is controlled via PI3K and JAK/STAT signaling. *Cell Death Dis* **7**, e2103 (2016).

61. Woehrl, B. *et al.* CXCL16 contributes to neutrophil recruitment to cerebrospinal fluid in pneumococcal meningitis. *J Infect Dis* **202**, 1389-1396 (2010).

62. Zhang, L. *et al.* Chemokine CXCL16 regulates neutrophil and macrophage infiltration into injured muscle, promoting muscle regeneration. *Am J Pathol* **175**, 2518-2527 (2009).

63. Besteman, S.B. *et al.* Transcriptome of airway neutrophils reveals an interferon response in life-threatening respiratory syncytial virus infection. *Clinical Immunology* **220**, 108593 (2020).

64. Ballesteros, I. *et al.* Co-option of Neutrophil Fates by Tissue Environments. *Cell* **183**, 1282-1297 e1218 (2020).

65. Yamada, M. *et al.* The increase in surface CXCR4 expression on lung extravascular neutrophils and its effects on neutrophils during endotoxin-induced lung injury. *Cell Mol Immunol* **8**, 305-314 (2011).

66. Bernhagen, J. *et al.* MIF is a noncognate ligand of CXC chemokine receptors in inflammatory and atherogenic cell recruitment. *Nature medicine* **13**, 587-596 (2007).

67. Pawig, L., Klasen, C., Weber, C., Bernhagen, J. & Noels, H. Diversity and Inter-Connections in the CXCR4 Chemokine Receptor/Ligand Family: Molecular Perspectives. *Front Immunol* **6**, 429 (2015).

68. Rodrigues, D.A.S. *et al.* CXCR4 and MIF are required for neutrophil extracellular trap release triggered by Plasmodium-infected erythrocytes. *PLoS pathogens* **16**, e1008230 (2020).

69. Adrover, J.M. *et al.* A neutrophil timer coordinates immune defense and vascular protection. *Immunity* **50**, 390-402 (2019).

70. Casanova-Acebes, M. *et al.* Rhythmic modulation of the hematopoietic niche through neutrophil clearance. *Cell* **153**, 1025-1035 (2013).

71. Ng, L.G., Ostuni, R. & Hidalgo, A. Heterogeneity of neutrophils. *Nature Reviews Immunology* **19**, 255-265 (2019).

72. Neidleman, J. *et al.* Distinctive features of SARS-CoV-2-specific T cells predict recovery from severe COVID-19. *medRxiv* (2021).

73. Group, R.C. Dexamethasone in hospitalized patients with Covid-19. *New England Journal of Medicine* **384**, 693-704 (2021).

74. Ronchetti, S., Ricci, E., Migliorati, G., Gentili, M. & Riccardi, C. How glucocorticoids affect the neutrophil life. *International journal of molecular sciences* **19**, 4090 (2018).

75. Mullard, A. Anti-IL-6Rs falter in COVID-19. *Nat Rev Drug Discov* **19**, 577 (2020).

76. Eddins, D.J. *et al.* Inactivation of SARS Coronavirus 2 and COVID-19 patient samples for contemporary immunology studies. *bioRxiv* (2021).

77. Beigel, J.H. *et al.* Remdesivir for the Treatment of Covid-19 - Final Report. *N Engl J Med* **383**, 1813-1826 (2020).

78. Orlov, M. *et al.* Endotracheal aspirates contain a limited number of lower respiratory tract immune cells. *Critical Care* **25**, 1-3 (2021).

79. Seren, S. *et al.* Proteinase release from activated neutrophils in mechanically ventilated patients with non-COVID-19 and COVID-19 pneumonia. *Eur Respir J* **57** (2021).

80. Dobin, A. *et al.* STAR: ultrafast universal RNA-seq aligner. *Bioinformatics* **29**, 15-21 (2013).

81. Hao, Y. *et al.* Integrated analysis of multimodal single-cell data. *bioRxiv* (2020).

82. Babcock, B.R., Kosters, A., Yang, J., White, M.L. & Ghosn, E. Data Matrix Normalization and Merging Strategies Minimize Batch-specific Systemic Variation in scRNA-Seq Data. *bioRxiv* (2021).

83. Mulè, M.P., Martins, A.J. & Tsang, J.S. Normalizing and denoising protein expression data from droplet-based single cell profiling. *bioRxiv* (2020).

84. Petukhov, V. *et al.* dropEst: pipeline for accurate estimation of molecular counts in droplet-based single-cell RNA-seq experiments. *Genome Biol* **19**, 78 (2018).

85. Zhou, Y. *et al.* Metascape provides a biologist-oriented resource for the analysis of systems-level datasets. *Nat Commun* **10**, 1523 (2019).

86. Lu, R. *et al.* Genomic characterisation and epidemiology of 2019 novel coronavirus: implications for virus origins and receptor binding. *Lancet* **395**, 565-574 (2020).

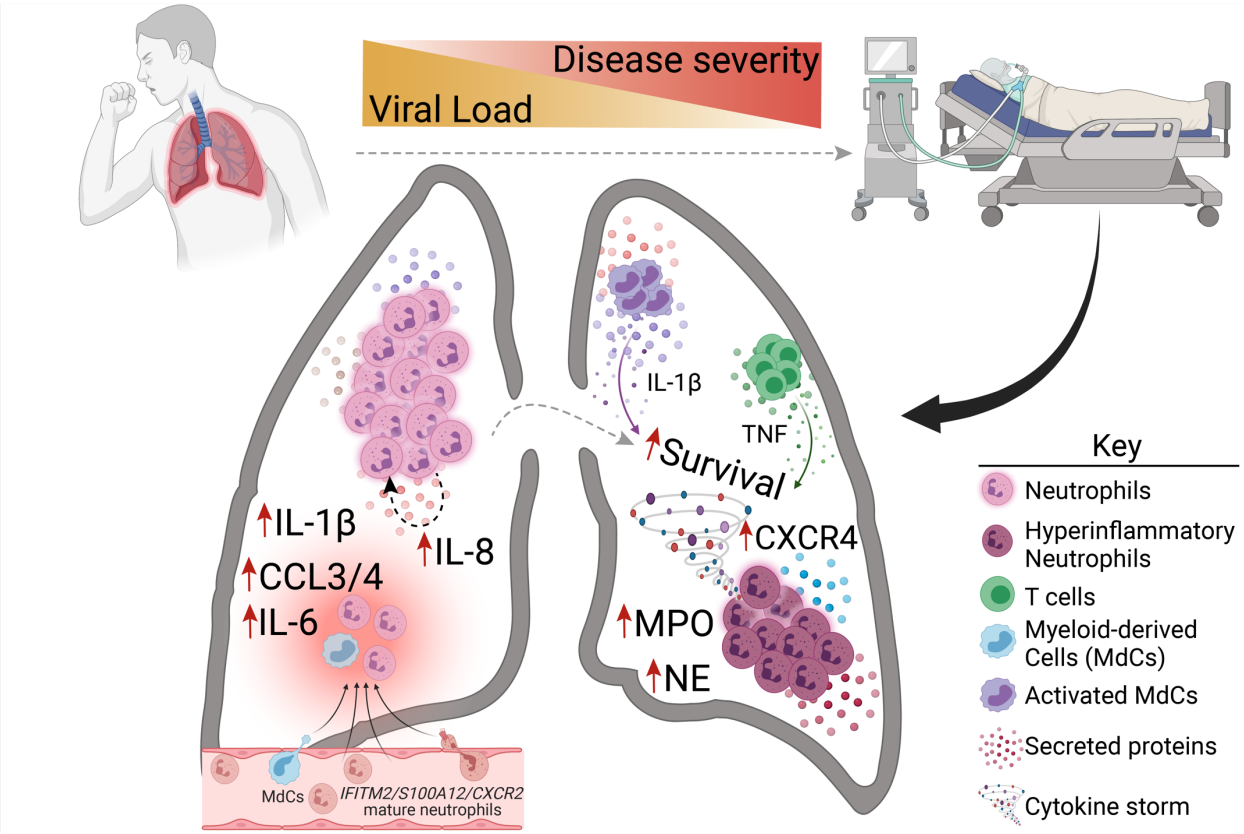

Graphical Abstract

The lung pathology due to severe COVID-19 is marked by a perpetual pathogenic neutrophilia, leading to acute respiratory distress syndrome (ARDS) even in the absence of viral burden. Circulating mature neutrophils are recruited to the airways via IL-8 (CXCL8)/CXCR2 chemotaxis. Recently migrated neutrophils further differentiate into a transcriptionally active and hyperinflammatory state, with an exacerbated expression of IL-8 (*CXCL8*), IL-1β (*IL1B*), *CCL3*, *CCL4*, neutrophil elastase (NE), and myeloperoxidase (MPO) activity. Airway neutrophils and recruited inflammatory monocytes further increase their production of IL-8 (*CXCL8*), perpetuating lung neutrophilia in a feedforward loop. MdCs and T cells produce IL-1β and TNF, driving neutrophils reprogramming and survival.

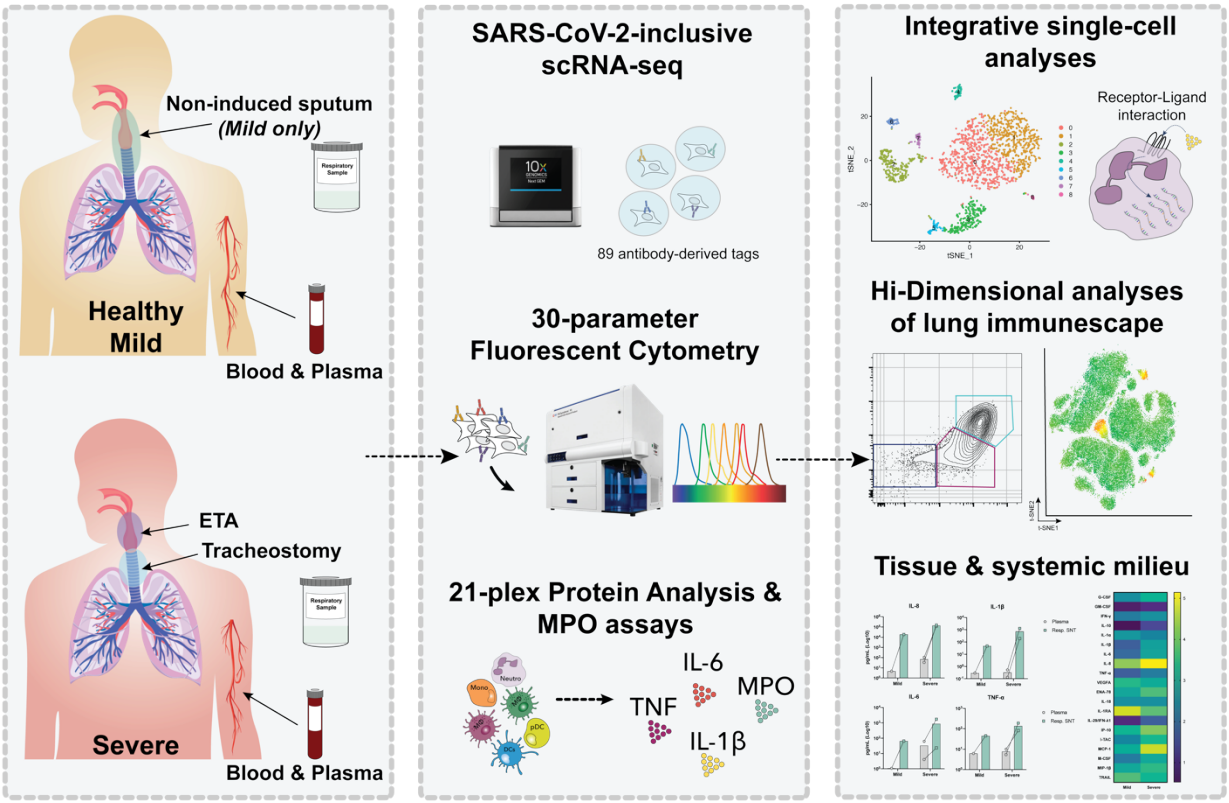

Figure 1. ***Experimental design for the systems immunology approach (integrated multi-omics single-cell assays) to study COVID-19 patient samples***. Respiratory samples (sputum or endotracheal aspirates) and matching blood from all subjects were collected for analysis by 21-plex Mesoscale analysis, high-dimensional (Hi-D) 30-parameter flow cytometry, and multi-omics scRNA-seq. Cells from endotracheal aspirates (ETA) and blood of severe COVID-19 patients along with blood from healthy individuals were surface-stained with a panel of 89 oligo-conjugated monoclonal antibodies before single-cell encapsulation, and analyses were performed with a custom human reference genome that included the SARS-CoV-2 genome to simultaneously detect viral mRNA transcripts. Integrative multi-omics analyses were performed on the resulting data sets.

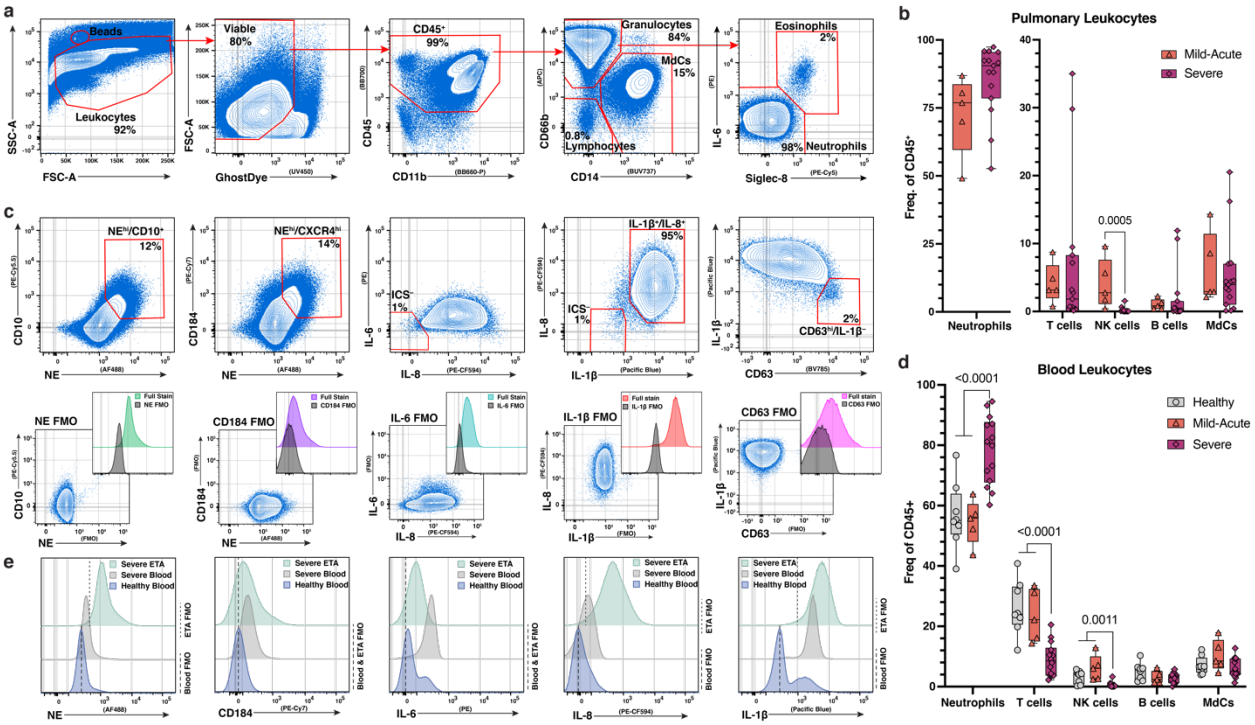

Figure 2. ***Exacerbated neutrophilia in the airways and matching blood of severe COVID-19 patients.*** (a) Representative gating strategy for all samples (see Extended Data Fig. 1 for full gating strategy). (b) Box plots show distributions of leukocytes isolated from endotracheal aspirates (ETA). (c) Representative plots demonstrating inflammatory profile of pulmonary neutrophils including neutrophil elastase (NE), CD184 (CXCR4), and intracellular staining of IL-6, IL-8, and IL-1β including the full stain and fluorescence minus one (FMO) controls (d) Box plots show distributions of leukocytes isolated from whole blood from severe patients. (e) Representative histograms showing median fluorescence intensity (MFI) of key markers across healthy blood (blue), severe blood (gray), and severe ETA (green) samples. MdCs = myeloid-derived cells. For comparisons across the three patient groups (i.e., healthy, mild-acute, severe), ordinary one-way ANOVA (if equal variance) or Brown-Forsythe and Welch ANOVA (if unequal variance) tests were performed for data with a normal distribution. Data with a lognormal distribution were analyzed with a Kruskal-Wallis test.

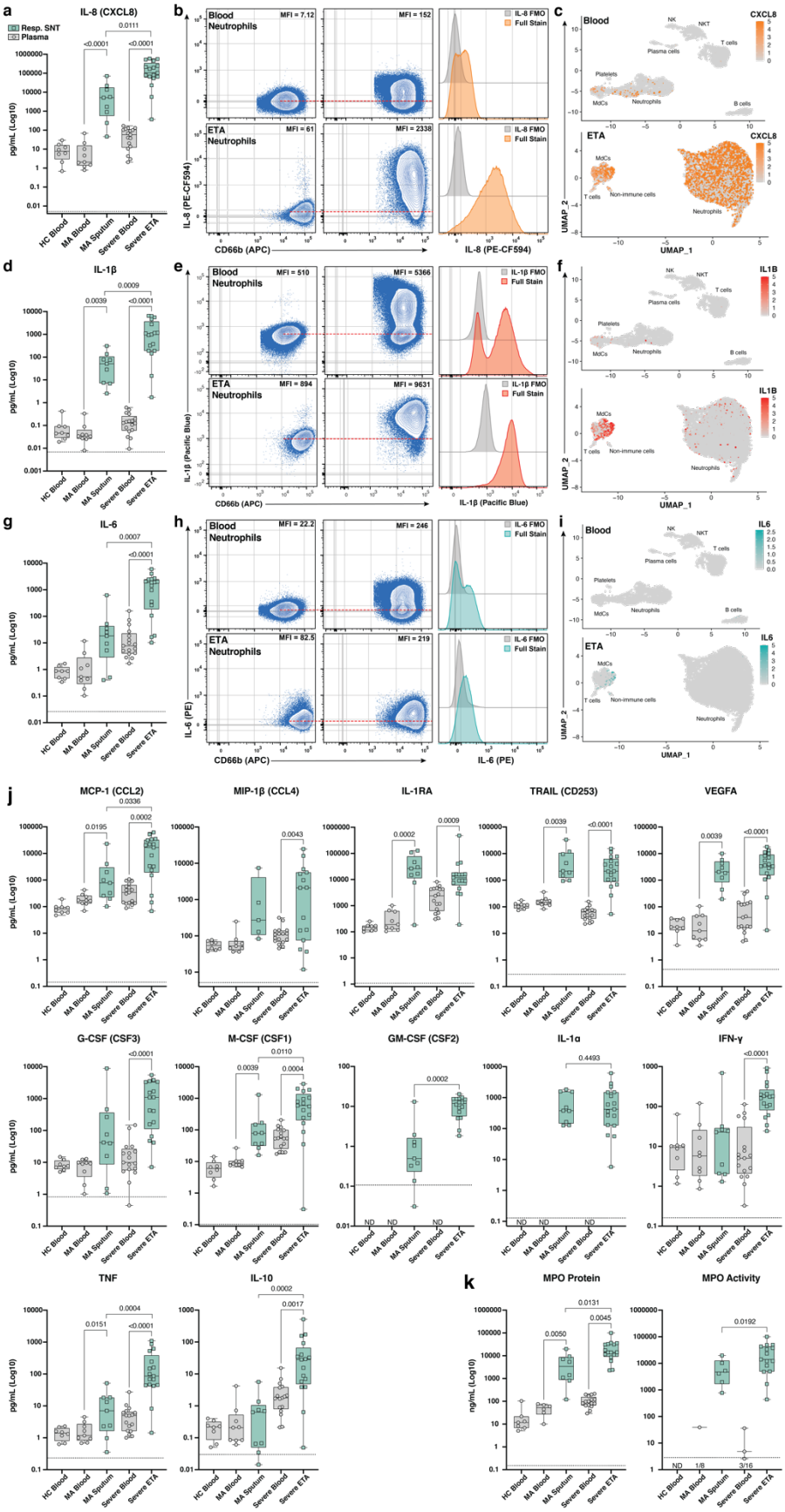
a
IL-8 (CXCL8)
Resp. SNT
Plasma
pg/mL (Log10)
HC Blood
MA Blood
MA Sputum
Severe Blood
Severe ETA
b
Blood
Neutrophils
ETA
Neutrophils
IL-8 FMO
Full Stain
IL-8 (PE-CF594)
CD66b (APC)
c
Blood
ETA
CXCL8
UMAP_1
UMAP_2
d
IL-1β
e
IL-1β FMO
IL-1β (Pacific Blue)
f
IL1B
g
IL-6
h
IL-6 FMO
IL-6 (PE)
i
IL6
j
MCP-1 (CCL2)
MIP-1β (CCL4)
IL-1RA
TRAIL (CD253)
VEGFA
G-CSF (CSF3)
M-CSF (CSF1)
GM-CSF (CSF2)
IL-1α
IFN-γ
TNF
IL-10
k
MPO Protein
MPO Activity
ng/mL (Log10)

1066

1067 **Figure 3**. ***Cytokine release syndrome is dominated by IL-8 and IL-1β with pronounced***
1068 ***myeloperoxidase content and activity in the lung microenvironment***. (a, d, g, j)
1069 Concentration (pg/mL) of 15 analytes interrogated by Mesoscale analyses in plasma (gray
1070 circles) and respiratory supernatant (Resp. SNT; green squares) from healthy control (HC),
1071 mild-acute (MA), and severe COVID-19 patients. (b, e, h) Representative flow cytometric
1072 intracellular staining for IL-8 (CXCL8), IL-1β, and IL-6, including the full stain and fluorescence
1073 minus one (FMO) controls in both blood and ETA neutrophils ($CD66b^+$). (c, f, i) UMAP
1074 visualizations of *CXCL8* (IL-8), *IL1B*, and *IL6*, which were also measured by intracellular flow
1075 cytometry staining and Mesoscale in both blood and ETA. (k) Concentration (ng/mL) of
1076 myeloperoxidase (MPO) protein and MPO activity in plasma vs. Resp. SNT. In (a, d, g, j, k),
1077 black dotted line = median lower limit of detection (LLOD) for assays (see Extended Data Table
1078 3). In (b, e, h) red dashed line indicates the median fluorescence intensity (MFI) of neutrophils in
1079 the FMO control (value listed in the plot).
1080

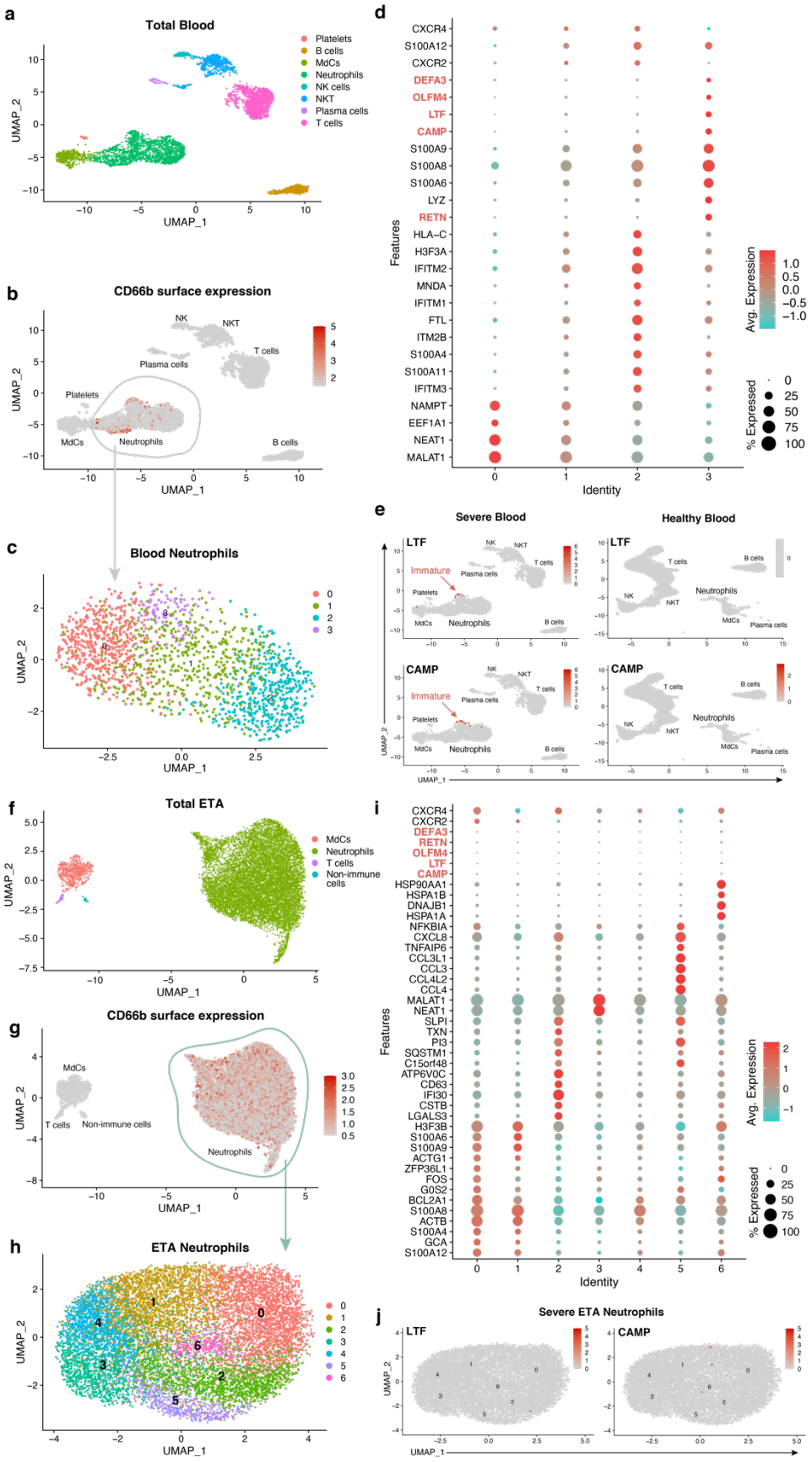
a
Total Blood
Platelets
B cells
MdCs
Neutrophils
NK cells
NKT
Plasma cells
T cells
UMAP_1
UMAP_2
b
CD66b surface expression
NK
NKT
T cells
Plasma cells
Platelets
MdCs
Neutrophils
B cells
c
Blood Neutrophils
d
Features
Identity
Avg. Expression
% Expressed
e
Severe Blood
Healthy Blood
LTF
CAMP
Immature
f
Total ETA
MdCs
Neutrophils
T cells
Non-immune cells
g
CD66b surface expression
h
ETA Neutrophils
i
Features
Identity
Avg. Expression
% Expressed
j
Severe ETA Neutrophils
LTF
CAMP

1081

1082 **Figure 4.** ***Multi-omic single-cell RNA-seq reveals emergency granulopoiesis in the***
1083 ***circulation and abundant heterogeneous populations of mature neutrophils in the***
1084 ***airways with distinct inflammatory states.*** UMAP visualization of scRNA-seq of total
1085 integrated blood (a) and endotracheal aspirate (ETA) (f) cells. Neutrophils were identified based
1086 on cell-surface markers (b and g), and total neutrophils were subclustered for further analysis (c
1087 and h). Dot plots of the intersection of the top differentially expressed genes in neutrophil
1088 clusters (d and i) sorted by average log-fold change for blood (d) and lung (i) neutrophils,
1089 respectively. UMAP visualization of signature genes of immature neutrophils (highlighted in d
1090 and i) in blood from severe patients compared to healthy individuals (e) and lungs of severe
1091 patients (j).
1092

1093

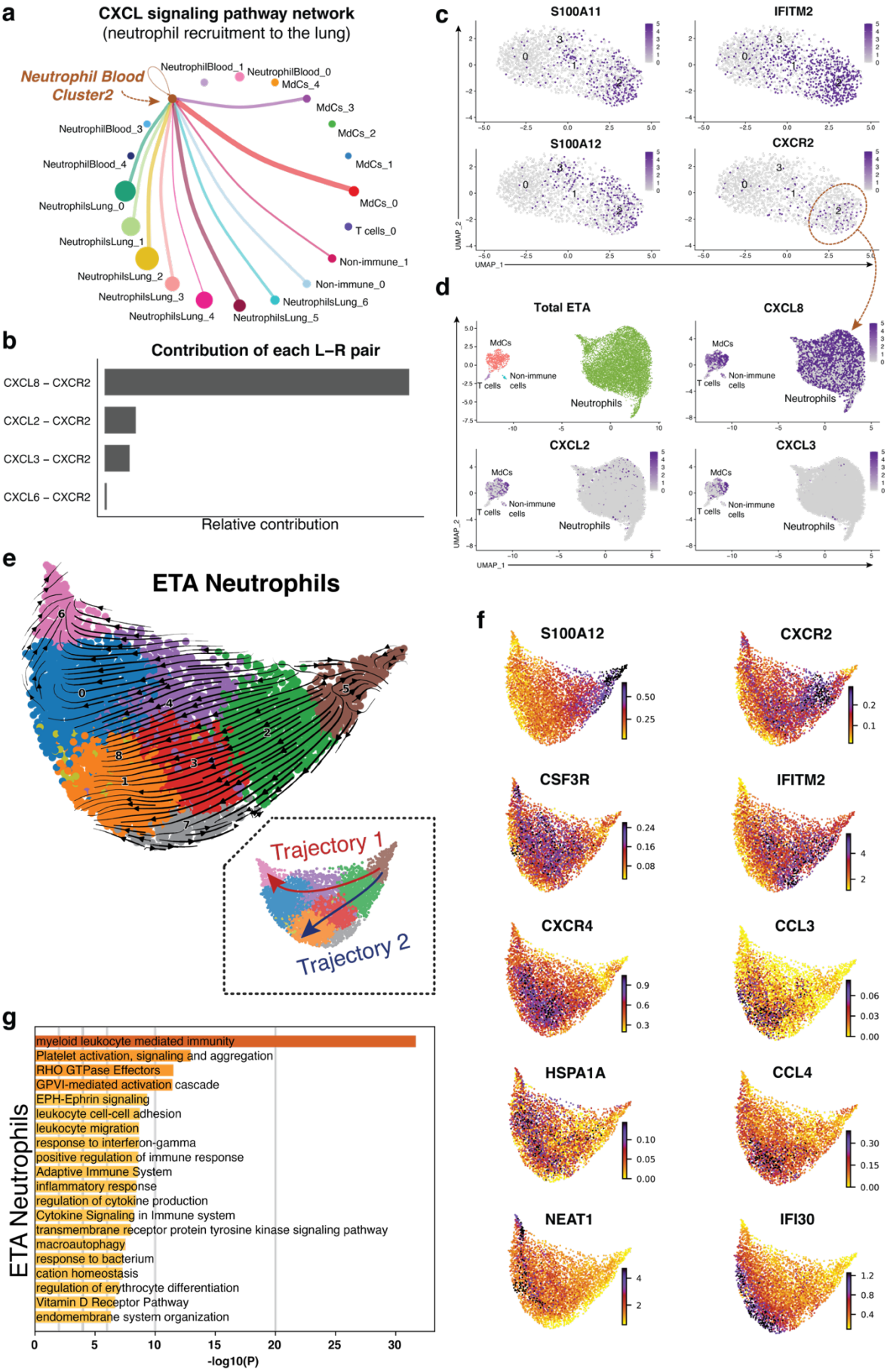
a
CXCL signaling pathway network
(neutrophil recruitment to the lung)
Neutrophil Blood Cluster2
NeutrophilBlood_1
NeutrophilBlood_0
MdCs_4
MdCs_3
MdCs_2
MdCs_1
MdCs_0
T cells_0
Non-immune_1
Non-immune_0
NeutrophilsLung_6
NeutrophilsLung_5
NeutrophilsLung_4
NeutrophilsLung_3
NeutrophilsLung_2
NeutrophilsLung_1
NeutrophilsLung_0
NeutrophilBlood_4
NeutrophilBlood_3
b
Contribution of each L–R pair
CXCL8 – CXCR2
CXCL2 – CXCR2
CXCL3 – CXCR2
CXCL6 – CXCR2
Relative contribution
c
S100A11
IFITM2
S100A12
CXCR2
UMAP_1
UMAP_2
d
Total ETA
CXCL8
CXCL2
CXCL3
MdCs
T cells
Non-immune cells
Neutrophils
e
ETA Neutrophils
Trajectory 1
Trajectory 2
f
S100A12
CXCR2
CSF3R
IFITM2
CXCR4
CCL3
HSPA1A
CCL4
NEAT1
IFI30
g
ETA Neutrophils
myeloid leukocyte mediated immunity
Platelet activation, signaling and aggregation
RHO GTPase Effectors
GPVI-mediated activation cascade
EPH-Ephrin signaling
leukocyte cell-cell adhesion
leukocyte migration
response to interferon-gamma
positive regulation of immune response
Adaptive Immune System
inflammatory response
regulation of cytokine production
Cytokine Signaling in Immune system
transmembrane receptor protein tyrosine kinase signaling pathway
macroautophagy
response to bacterium
cation homeostasis
regulation of erythrocyte differentiation
Vitamin D Receptor Pathway
endomembrane system organization
-log10(P)

1094 **Figure 5**. ***Mature neutrophils are continuously recruited from circulation and progress***
1095 ***toward a hyperinflammatory state***. Cell receptor-ligand pair analyses (CellChat[31]) from
1096 scRNA-seq data identify significant CXCL signaling pathway network enrichment between lung
1097 cells and blood neutrophils (a and b). Blood neutrophil cluster 2 represents the main subset
1098 potentially recruited to the lung (a). Recruitment of blood cluster 2 (a and c) is largely
1099 orchestrated by the CXCL8 (IL-8)/CXCR2 axis, and to a lesser extent, by the CXCL2 and
1100 CXCL3 (b and d). *S100A11/12, IFITM2,* and *CXCR2* mark a cluster of mature neutrophils in the
1101 blood (c) that likely represents the neutrophil subset recruited to the lung (d). Cell trajectory
1102 analysis (scVelo[32]) identifies two potential pathways (Trajectories 1 and 2) for recently migrated
1103 neutrophils (e), that begin with a gene signature consistent with neutrophil blood cluster 2 (c and
1104 f). Neutrophils recruited to the lung acquire a hyperinflammatory profile along Trajectory 2 (e
1105 and f), characterized by high expression of interferon-stimulated gene (ISG) *IFI30* along with
1106 macrophage inflammatory proteins *CCL3* (MIP-1α) and *CCL4* (MIP-1β), whereas *CSF3R* and
1107 *CXCR4* are increased in cells along both trajectories (f). Neutrophils along Trajectory 1 may
1108 reflect cells progressing to apoptosis expressing higher levels of *HSPA1A* (HSP70) followed by
1109 *NEAT1* (f). Pathway and process enrichment analyses performed in Metascape[85] reveals that
1110 myeloid-mediated immunity and platelet activation, signaling, and aggregation are significantly
1111 enriched in neutrophils in the lungs of severe patients (g). MdCs: Myeloid-derived Cells.
1112

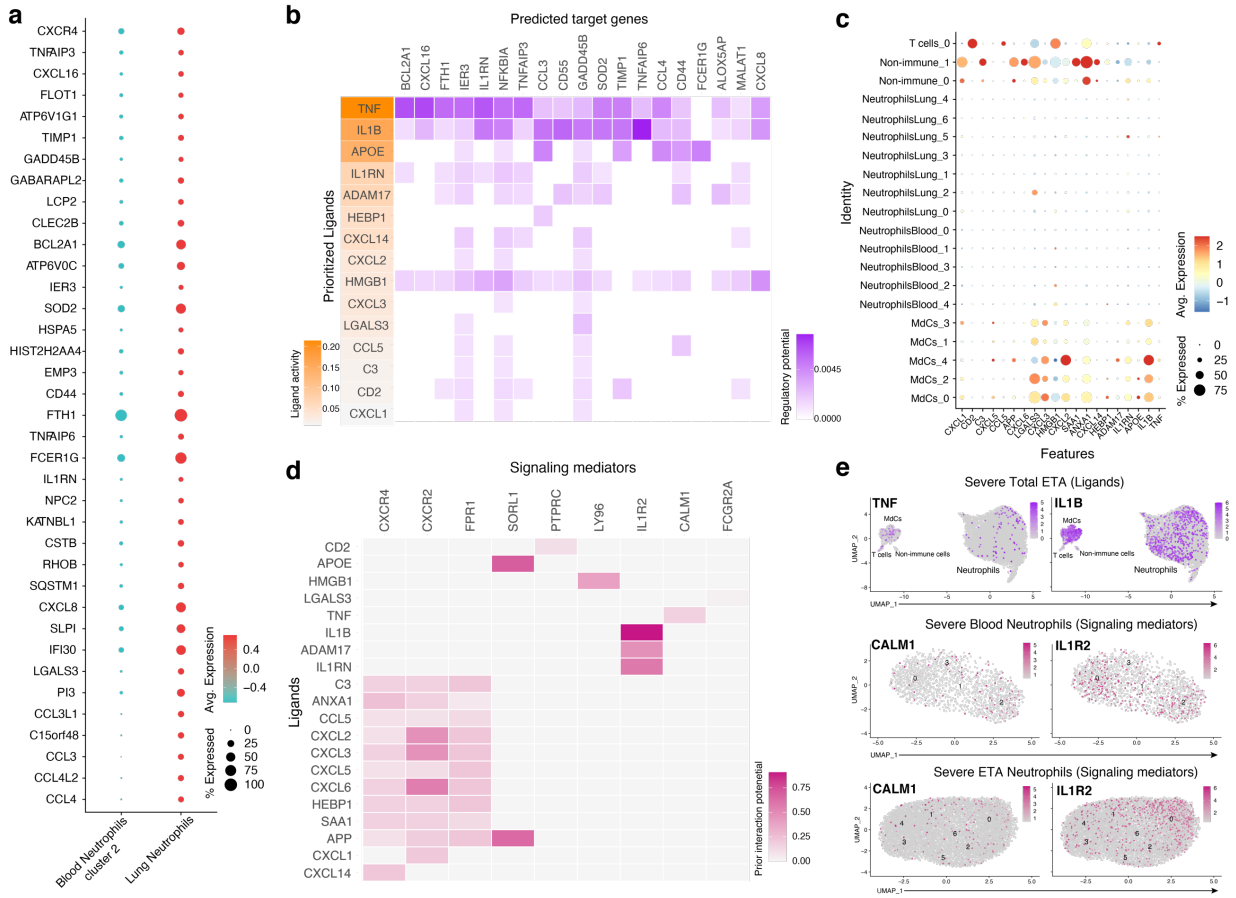

Figure 6. ***TNF and IL-1β drive inflammatory program in neutrophils recruited to the lung.*** (a) Dot plots showing 37 of the 67 differentially expressed genes in lung neutrophils versus blood neutrophil cluster 2 sorted by average log-fold change used as input for NicheNet[38] analyses (b) NicheNet[38] analyses identified the highest prioritized ligands (top 15) ordered by ligand activity (y-axis) that best predict the pulmonary neutrophil gene signature (x-axis). The predicted target genes represent the pulmonary neutrophil gene signature identified by differential gene expression analysis between blood neutrophils from cluster 2 and ETA neutrophils (see Extended Data Fig. 5d) (b) Dot plots of the intersection of the top 15 expressed prioritized ligands from all cells in the ETA samples. (c) Ligand-receptor matrix of putative signaling mediators for the top 15 prioritized ligands identified in (a). (d) UMAP visualizations of *TNF* and *IL1B* transcripts in the total ETA along with expression of predicted signaling mediators in blood (middle) and ETA (bottom) neutrophils from severe patients.

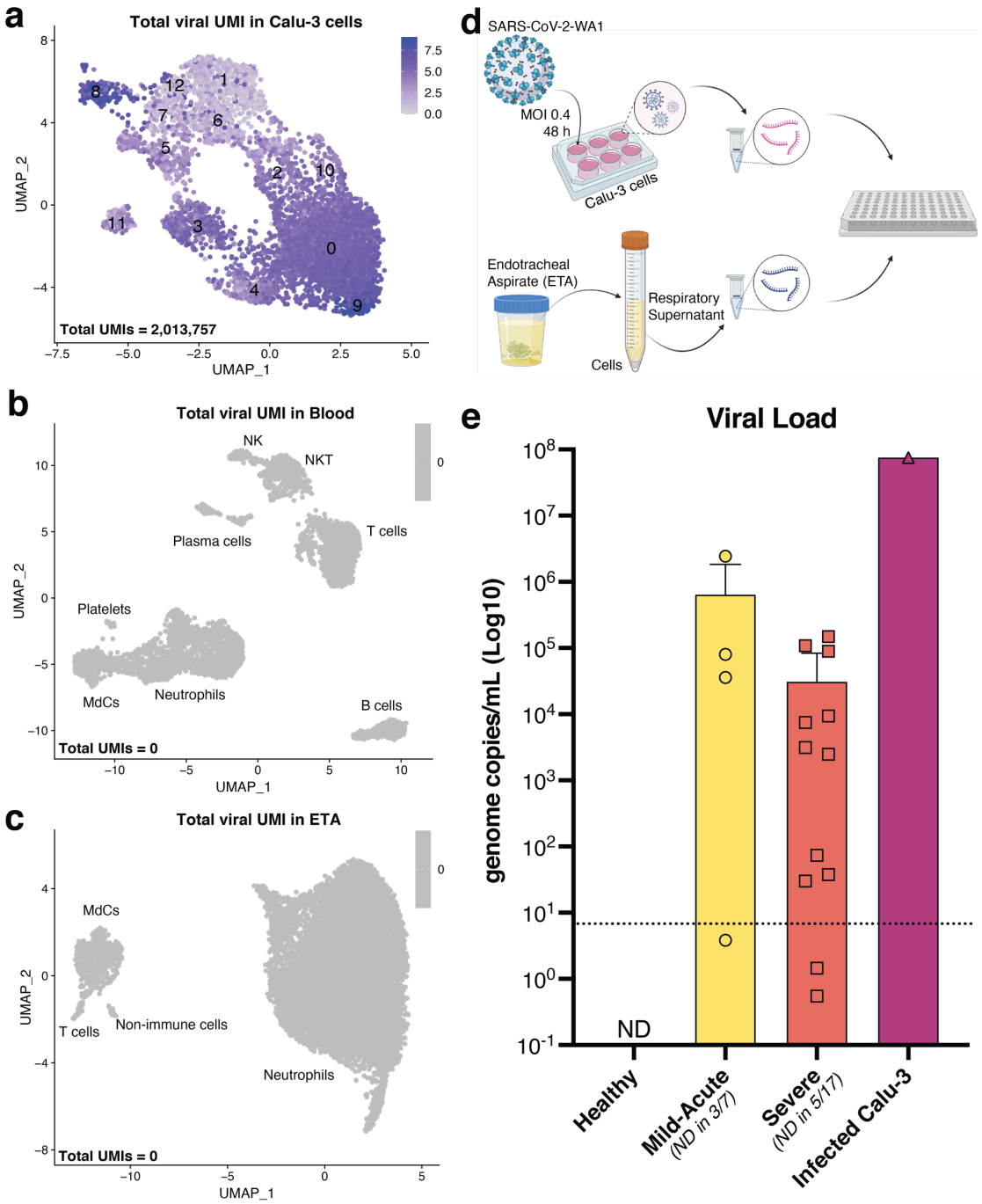

Figure 7. ***Viral transcripts (scRNA-seq) and viral load in the airways of severe patients.*** Calu-3 cells infected with SARS-CoV-2 USA-WA1/2020 (MOI 0.4) were encapsulated for scRNA-seq assays (a) following the same protocol used for patient cells from blood (b) and ETA (c). Millions of viral transcripts (or unique molecular identifiers; UMIs) were detected in about 5,000 Calu-3 cells (a), but not in the cells from severe patients (total UMI = 0; b and c). RT-qPCR (d) results of culture supernatant from Calu-3 infected cells and respiratory supernatants from mild-acute and severe patients (e) show a lower viral load in severe patients than in mild-acute patients and in the Calu-3-infected culture supernatant. ND = not detected; horizontal dotted line = lower limit of detection (LLOD).

1138 **Supplemental Material:**

#	Demographic	PID	Status	Sex	Age Group	Dexamethasone or equivalent	Remdesivir (No. of doses)	Date PCR positive Dx	Date intubated	Date sample collected	Length ICU stay (days)	Clinical Outcome
1	AA	PHA0001	Severe	Male	35-54	Yes	0	6/9/2020	6/8/2020	6/17/2020	32	Recovered
2	AA	PHA0004	Severe	Male	35-54	Yes	0	7/11/2020	7/18/2020	8/5/2020	37	Recovered
3	AA	PHA0006	Severe	Male	35-54	Yes	0	8/11/2020	8/16/2020	8/20/2020	8	Recovered
4	AA	PHA0018	Severe	Male	35-54	Yes	2	10/14/2020	9/29/2020	10/8/2020	13	Recovered
5	AA	PHA0041	Severe	Male	35-54	Yes	2	2/6/2021	2/6/2021	2/10/2021	14	Recovered
6	AA	PHA0003	Severe	Male	55+	Yes	2	6/23/2020	6/25/2020	6/30/2020	14	Succumbed
7	A	PHA0008	Severe	Male	55+	Yes	2	8/29/2020	8/30/2020	9/3/2020	19	Recovered
8	AA	PHA0024	Severe	Male	55+	Yes	2	12/27/2020	12/31/2020	1/6/2021	9	Recovered
9	AA	PHA0025	Severe	Male	55+	Yes	0	12/20/2020	12/24/2020	1/8/2021	26	Recovered
10	AA	PHA0031	Severe	Male	55+	Yes	1	1/23/2021	1/24/2021	1/27/2021	11	Succumbed
11	AA	PHA0032	Severe	Male	55+	Yes	1	1/9/2021	1/14/2020	1/27/2021	40	Recovered
12	AA	PHA0035	Severe	Male	55+	Yes	0	1/18/2021	1/20/2021	2/2/2021	53	Recovered
13	AA	PHA0036	Severe	Female	18-34	Yes	2	1/10/2021	12/31/2020	2/2/2021	42	Recovered
14	AA	PHA0002	Severe	Female	55+	Yes	0	6/20/2020	6/20/2020	6/24/2020	25	Recovered
15	AA	PHA0005	Severe	Female	55+	Yes	0	7/16/2020	7/18/2020	8/12/2020	33	Recovered
16	AA	PHA0007	Severe	Female	55+	Yes	0	8/9/2020	8/10/2020	9/2/2020	60	Recovered
17	AA	PHA0010	Severe	Female	55+	Yes	2	9/17/2020	9/21/2020	9/24/2020	18	Recovered
18	AA	PHA0026	Severe	Female	55+	Yes	1	12/27/2020	12/28/2020	1/8/2021	16	Succumbed
19	A	PHA0040	Mild-Acute	Male	35-54	Yes	0	1/6/2021	N/A	2/8/2021	N/A	Recovered
20	AA	PHA0043	Mild-Acute	Male	35-54	Yes	0	Unclear	N/A	2/18/2021	N/A	Recovered
21	AA	PHA0023	Mild-Acute	Male	55+	Yes	0	11/6/2020	N/A	11/11/2020	N/A	Recovered
22	AA	PHA0047	Mild-Acute	Male	55+	Yes	0	2/8/2021	N/A	2/19/2021	N/A	Recovered
23	AA	PHA0012	Mild-Acute	Female	35-54	Yes	0	9/18/2020	N/A	9/29/2020	N/A	Recovered
24	AA	PHA0013	Mild-Acute	Female	35-54	Yes	0	9/21/2020	N/A	9/29/2020	N/A	Recovered
25	AA	PHA0044	Mild-Acute	Female	35-54	Yes	0	2/16/2021	N/A	2/19/2021	N/A	Recovered
26	AA	PHA0046	Mild-Acute	Female	35-54	Yes	0	2/12/2021	N/A	2/19/2021	N/A	Recovered
27	AA	PHA0045	Mild-Acute	Female	55+	Yes	0	2/12/2021	N/A	2/19/2021	N/A	Recovered
28	AA	PHA1009	Healthy	Female	18-34	Yes	0	N/A	N/A	10/23/2020	N/A	N/A
29	AA	PHA1005	Healthy	Female	35-54	Yes	0	N/A	N/A	10/23/2020	N/A	N/A
30	AA	PHA1006	Healthy	Female	35-54	Yes	0	N/A	N/A	10/23/2020	N/A	N/A
31	AA	PHA1007	Healthy	Female	35-54	Yes	0	N/A	N/A	10/23/2020	N/A	N/A
32	AA	PHA1008	Healthy	Female	35-54	Yes	0	N/A	N/A	10/23/2020	N/A	N/A
33	AA	PHA1010	Healthy	Female	35-54	Yes	0	N/A	N/A	10/23/2020	N/A	N/A
34	AA	PHA1011	Healthy	Female	35-54	Yes	0	N/A	N/A	2/10/2021	N/A	N/A
35	AA	PHA1012	Healthy	Female	55+	Yes	0	N/A	N/A	2/17/2021	N/A	N/A

1139

1140 **Extended Data Table 1.** ***Demographic and clinical data from the 35 Black/African***
1141 ***American individuals enrolled in our studies.*** Table describing demography, status, sex, and
1142 age of study participants along with select details of clinical course including administration of
1143 Dexamethasone and Remdesivir, date first intubated (severe, ICU patients only), date of PCR
1144 positive diagnosis (Dx), date clinical specimens were collected, and total length ICU stay in
1145 days, and clinical outcome (whether recovered or succumbed to disease).
1146

Characteristics	All subjects (*N* = 35)		
	Healthy (*N* = 8)	**Mild-Acute** (*N*=9)	**Severe** (*N*=18)
Age			
A. Mean age ± SD	46 ± 11	51 ± 12	56 ± 14
B. Age range	31 – 70	35 – 68	22 – 81
Gender			
A. Female	8 (100%)	5 (56%)	6 (33%)
B. Male	0 (0%)	4 (44%)	12 (67%)
Site of endotracheal aspiration			
A. Endotracheal tube	—	—	9 (50%)
B. Tracheostomy	—	—	9 (50%)
Medical History			
A. Smoking History			
i) Never	7 (87.5%)	7 (78%)	12 (67%)
ii) Former	1 (12.5%)	2 (22%)	2 (11%)
iii) Current	0 (0%)	0 (0%)	4 (22%)
B. Hypertension (HTN)	3 (37.5%)	3 (33%)	11 (61%)
C. Obesity	2 (25%)	1 (11%)	4 (22%)
D. Asthma	2 (25%)	2 (22%)	2 (11%)
E. COPD	0 (0%)	0 (0%)	2 (11%)
F. Diabetes mellitus (DM)			
i) Type I DM	0 (0%)	0 (0%)	0 (0%)
ii) Type II DM	1 (12.5%)	0 (0%)	8 (44%)
G. Deep vein thrombosis (DVT)	0 (0%)	0 (0%)	1 (5%)
H. Hypothyroidism	0 (0%)	0 (0%)	1 (5%)
I. Congestive Heart Failure (CHF)	1 (12.5%)	0 (0%)	5 (28%)
J. Gastroesophegeal reflux disease (GERD)	1 (12.5%)	1 (11%)	1 (5%)
K. Dyslipidemia	0 (0%)	1 (11%)	1 (5%)
L. Obstructive sleep apnea (OSA)	0 (0%)	0 (0%)	2 (11%)
M. Coronary artery disease (CAD)	0 (0%)	0 (0%)	1 (5%)
N. Chronic kidney disease	0 (0%)	1 (11%)	1 (5%)
O. Cancer	0 (0%)	0 (0%)	0 (0%)
P. Autoimmune hemolytic anemia	0 (0%)	0 (0%)	1 (5%)
Q. Thrombocytopenia	0 (0%)	0 (0%)	1 (5%)
R. Athritis/Rheumatoid arthritis (RA)	1 (12.5%)	0 (0%)	1 (5%)
Complications			
A. Acute respiratory distress syndrome (ARDS)	—	—	18 (100%)
B. Hypoxemic respiratory failure	—	—	13 (72%)
C. Extracorpeal membrane oxygenation (ECMO)	—	—	2 (11%)
D. Shock	—	—	15 (83%)
E. Nosocomial pneumonia	—	—	6 (33%)
F. Coagulopathy	—	—	3 (17%)
G. Seizures	—	—	3 (17%)
H. Cardiac arrythmia	—	—	3 (17%)
I. Renal failure	—	—	8 (44%)
J. Renal replacement therapy	—	—	6 (33%)

1148 **Extended Data Table 2.** ***Clinical characteristics of the 35 Black/African American***
1149 ***individuals enrolled in our studies.*** Table describing clinical characteristics of 35 patients
1150 across the 3 cohorts (healthy, mild-acute, and severe) including age, gender, site of
1151 endotracheal aspiration (ETA), medical history, along with complications for the severe patients
1152 admitted to the ICU.
1153

1154

a CoV-Neutrophil

	Laser	Detector	Antigen	Fluorophore	Clone	Isotype	Vendor	Cat. No.	Titration
	488 nm	B 488/10	Side Scatter (SSC)	—	—	—	—	—	—
1		B 515/20	Neutrophil elastase (NE)	AF488	950318	Mouse IgG1, κ	R&D Systems	IC91671G	1:25
2		B 610/20	CD45-RA	BB630-P	HI-100	Mouse IgG2a, κ	BD Biosciences	624294	1:160
3		B 670/30	CD11b	BB660-P	ICRF44	Mouse IgG1, κ	BD Biosciences	624295	1:50
4		B 710/50	CD45	BB700	HI-30	Mouse IgG1, κ	BD Biosciences	746090	1:640
5		B 750/30	CD4	BB755-P	RPA-T4	Mouse IgG1, κ	BD Biosciences	624391	1:100
6		B 780/60	HLA-DR (MHC II)	BB790-P	G46-6	Mouse IgG2a, κ	BD Biosciences	624296	1:50
7	405 nm	V 431/28	CD163	BV421	GHI/6I	Mouse IgG1, κ	BioLegend	333612	1:25
8		V 470/15	IL-1β	Pacific Blue	H1b-98	Mouse IgG1, κ	BioLegend	511710	1:20
9		V 586/15	CD56	BV570	HCD56	Mouse IgG1, κ	BioLegend	318330	1:100
10		V 610/20	CD86 *	BV605	FUN-1	Mouse IgG1, κ	BD Biosciences	562999	1:50
11		V 670/30	TNF	BV650	MAb11	Mouse IgG1, κ	BD Biosciences	563418	1:80
12		V 710/50	CD19	BV711	HIB19	Mouse IgG1, κ	BioLegend	302246	1:20
13		V 740/35	CD16 (FcγRIII)	BV750	3G8	Mouse IgG1, κ	BD Biosciences	747461	1:320
14		V 780/60	CD63 (LAMP-3)	BV785	H5C6	Mouse IgG1, κ	BioLegend	353044	1:80
15	561 nm	YG 586/15	IL-6	PE	MQ2-13A5	Rat IgG1, κ	BD Biosciences	554545	1:20
16		YG 610/20	IL-8 (CXCL8)	PE-CF594	G265-8	Mouse IgG2b, κ	BD Biosciences	563531	1:20
17		YG 670/30	Siglec-8 *	PE-Cy5	7C9	Mouse IgG1, κ	BioLegend	347114	1:100
18		YG 710/50	CD10	PE-Cy5.5	HI10a	Mouse IgG1, κ	Homemade	—	1:40
19		YG 780/60	CD184 *	PE-Cy7	12G5	Mouse IgG2a, κ	BioLegend	306514	1:40
20	355 nm	UV 379/28	CD64 (FcγRI)	BUV395	10.1	Mouse IgG1, κ	BD Biosciences	740300	1:80
21		UV 450/50	GhostDye (Viability)	UV450	—	—	Tonbo Biosciences	13-0868-T500	1:100
22		UV 586/15	CD172a/b (SIRPα/β1)	BUV563	SE5A5	Mouse IgG1, κ	BD Biosciences	748435	1:10
23		UV 670/30	CD123 (IL-3Rα)	BUV661	9F5	Mouse IgG1, κ	BD Biosciences	741628	1:40
24		UV 740/35	CD14	BUV737	M5E2	Mouse IgG2a, κ	BD Biosciences	612763	1:50
25		UV 820/60	CD3ε	BUV805	SK1	Mouse IgG1, κ	BD Biosciences	612889	1:40
26	640 nm	R 670/30	CD66b	APC	QA17A51	Mouse IgG1, κ	BioLegend	396906	1:200
27		R 710/50	CD11c	AF700	Bu15	Mouse IgG1, κ	BioLegend	337220	1:200
28		R 780/60	CD32 (FcγRII)	APC-Fire750	FUN-2	Mouse IgG2b, κ	BioLegend	303220	1:400

* = alternate reagents used in panel iterations (see c below); -P denotes prototype reagents

b CoV-Global Distributions

	Laser	Detector	Antigen	Fluorophore	Clone	Isotype	Vendor	Cat. No.	Titration
	488 nm	B 488/10	Side Scatter (SSC)	—	—	—	—	—	—
1		B 515/20	CD45	AF488	HI-30	Mouse IgG1, κ	BioLegend	304017	1:160
2	405 nm	V 431/28	CD56	BV421	HCD56	Mouse IgG1, κ	BioLegend	318328	1:40
3		V 610/20	CD8α	BV605	SK1	Mouse IgG1, κ	BioLegend	344742	1:20
4		V 670/30	HLA-DR (MHC II)	BV650	L243	Mouse IgG2a, κ	BioLegend	307650	1:50
5		V 710/50	CD4	BV711	RPA-T4	Mouse IgG1, κ	BioLegend	300558	1:40
6		V 740/35	CD16 (FcγRIII)	BV750	3G8	Mouse IgG1, κ	BD Biosciences	747461	1:320
7		V 780/60	CD19	BV785	HIB19	Mouse IgG1, κ	BioLegend	302240	1:40
8	561 nm	YG 586/15	CD123 (IL-3Rα)	PE	6H6	Mouse IgG1, κ	BioLegend	306006	1:400
9		YG 670/30	Siglec-8	PE-Cy5	7C9	Mouse IgG1, κ	BioLegend	347114	1:100
10		YG 710/50	CD14	PE-Fire700	63D3	Mouse IgG1, κ	BioLegend	367158	1:100
11		YG 780/60	CD11c	PE-Cy7	Bu-15	Mouse IgG1, κ	BioLegend	337216	1:160
12	355 nm	UV 450/50	GhostDye (Viability)	UV450	—	—	Tonbo Biosciences	13-0868-T500	1:100
13	640 nm	R 670/30	CD11b	APC	ICRF44	Mouse IgG1, κ	BioLegend	301350	1:400
14		R 710/50	CD3ε	AF700	HIT3a	Mouse IgG2a, κ	BioLegend	300324	1:320
15		R 780/60	CD66b	APC-Fire750	QA17A51	Mouse IgG1, κ	BioLegend	396908	1:80

c Alternate Reagents

	Laser	Detector	Antigen	Fluorophore	Clone	Isotype	Vendor	Cat. No.	Titration
1	405 nm	V670/30	CD169 (Siglec-1)	BV605	7-239	Mouse IgG1, κ	BioLegend	346010	1:40
2		V670/30	CD182 (CXCR2)	BV605	6C6	Mouse IgG1, λ	BD Biosciences	744197	1:40
3	561 nm	YG 670/30	CD86	PE-Cy5	IT2.2	Mouse IgG1, κ	BioLegend	305408	1:20
4		YG 780/60	CD206 (MMR)	PE-Cy7	15-2	Mouse IgG2a, κ	BioLegend	321124	1:10

1155

1156 **Extended Data Table 3.** ***High-dimensional 30-parameter, including intracellular cytokine***
1157 ***staining, and 17-parameter flow cytometry panels used for airway and blood cells.*** Flow
1158 cytometer configuration and cytometry reagents used in the final panels to interrogate (a)
1159 neutrophil phenotype and (b) global immune cell distributions and blood and ETA samples.
1160 Channels marked with an asterisk (*) denote alternate reagents (c) used in earlier panel
1161 iterations for some samples in this study. Monoclonal antibody (mAb) master mixes were
1162 prepared in BD Horizon™ Brilliant Stain Buffer and samples stained as described in the
1163 methods section. Titrations of all reagents were determined in house for each lot independently
1164 prior to use. AF: AlexaFluor, APC: Allophycocyanin, BB: Brilliant Blue, BUV: Brilliant Ultraviolet,
1165 BV: Brilliant Violet, FITC: Fluorescein isothiocyanate, PE: Phycoerythrin. Fluorophores marked
1166 with -P denote prototype reagents and are custom conjugations from BD Biosciences.
1167

a

	Analyte	Median LLOD (pg/mL)	LLOD Range (pg/mL)
1	G-CSF (CSF3)	0.84 ± 0.88	0.15—2.12
2	GM-CSF (CSF2)	0.11 ± 0.13	0.01—0.31
3	IFN-γ	1.31 ± 1.12	0.16—2.79
4	IL-10	0.03 ± 0.02	0.01—0.06
5	IL-1α	0.13 ± 0.07	0.04—0.19
6	IL-1β	0.07 ± 0.05	0.01—0.12
7	IL-6	0.31 ± 0.39	0.03—0.89
8	IL-8 (CXCL8)	0.03 ± 0.03	0.02—0.08
9	TNF	0.24 ± 0.13	0.07—0.35
10	VEGFA	0.43 ± 0.44	0.06—1.06
11	ENA-78 (CXCL5)	0.15 ± 0.07	0.08—0.23
12	IL-18	1.02 ± 1.31	0.14—2.92
13	IL-1RA	1.08 ± 0.23	0.83—1.28
14	IL-29 (IFNλ1)	0.28 ± 0.11	0.13—0.38
15	IP-10 (CXCL10)	0.70 ± 0.99	0.18—2.19
16	I-TAC (CXCL11)	1.82 ± 0.23	1.59—2.13
17	MCP-1 (CCL2)	0.14 ± 0.05	0.09—0.21
18	M-CSF (CSF1)	0.10 ± 0.04	0.06—0.14
19	MIP-1β (CCL4)	5.17 ± 2.40	2.78—8.51
20	TRAIL (CD253)	0.28 ± 0.11	0.18—0.44
21	SDF1α (CXCL12)	30.13 ± 26.73	10.60—60.60

b

	Assay	Median LLOD (ng/mL)	LLOD Range (ng/mL)	Median LLOQ (ng/mL)	LLOQ Range (ng/mL)
1	Total MPO	0.15 ± 0.15	0.03—0.42	0.30 ± 0.30	0.05—0.84
2	MPO Activity	2.86 ± 1.98	0.38—6.03	5.72 ± 3.96	0.76—12.07

Extended Data Table 4. ***Mesoscale U-PLEX biomarker group 1 human and myeloperoxidase (MPO) assays.*** Median ± SD and range of lower limits of detection (LLOD) for (a) Mesoscale UPLEX analytes and (b) MPO assays. Lower limits of quantification (LLOQ; MPO assays) and LODs (determined by standard curve) were run for each assay plate independently and the median LLOD plotted as horizontal dotted lines for each assay (see Fig. 3 and Extended Data Fig. 2).

	Antigen	Clone	Vendor	Cat. No.		Antigen	Clone	Vendor	Cat. No.
1	CD10	HI10a	Biolegend	312233	**46**	CD324	67A4	Biolegend	324127
2	CD101 (BB27)	BB27	Biolegend	331017	**47**	CD326 (EpCAM)	9C4	Biolegend	324247
3	CD103 (Integrin αE)	Ber-ACT8	Biolegend	350233	**48**	CD335 (NKp46)	9.00E+02	Biolegend	331941
4	CD107a (LAMP-1)	H4A3	Biolegend	328649	**49**	CD370 (CLEC9A)	8F9	Biolegend	353809
5	CD117 (c-kit)	104D2	Biolegend	313243	**50**	CD38	HIT2	Biolegend	303543
6	CD11b	ICRF44	Biolegend	301359	**51**	CD4	RPA-T4	Biolegend	300567
7	CD11c	S-HCL-3	Biolegend	371521	**52**	CD40	5C3	Biolegend	334348
8	CD123 (IL-3Rα)	6H6	Biolegend	306045	**53**	CD41	HIP8	Biolegend	303739
9	CD127 (IL-7Rα)	A019D5	Biolegend	351356	**54**	CD44	BJ18	Biolegend	338827
10	CD133	S16016B	Biolegend	394007	**55**	CD45	2D1	Biolegend	368545
11	CD137	4B4-1	Biolegend	309839	**56**	CD45R	RA3-6B2	Biolegend	103273
12	CD138 (Syndecan-1)	MI15	Biolegend	356539	**57**	CD45RA	HI100	Biolegend	304163
13	CD14	M5E2	Biolegend	301859	**58**	CD45RO	UCHL1	Biolegend	304259
14	CD15 (SSEA-1)	W6D3	Biolegend	323053	**59**	CD49a	TS2/7	Biolegend	328319
15	CD16 (FcγRIII)	3G8	Biolegend	302065	**60**	CD5	UCHT2	Biolegend	300637
16	CD161	HP-3G10	Biolegend	339947	**61**	CD56 (NCAM)	QA17A16	Biolegend	392425
17	CD163	GHI/61	Biolegend	333637	**62**	CD62L	DREG-56	Biolegend	304851
18	CD169	7-239	Biolegend	346021	**63**	CD64 (FcγRI)	10.1	Biolegend	305045
19	CD183 (CXCR3)	G025H7	Biolegend	353747	**64**	CD66b	6/40c	Biolegend	392909
20	CD184 (CXCR4)	12G5	Biolegend	306533	**65**	CD69	FN50	Biolegend	310951
21	CD185 (CXCR5)	J252D4	Biolegend	356939	**66**	CD80	2D10	Biolegend	305243
22	CD19	HIB19	Biolegend	302265	**67**	CD86	IT2.2	Biolegend	305447
23	CD196 (CCR6)	G034E3	Biolegend	353440	**68**	CD8α	RPA-T8	Biolegend	301071
24	CD197 (CCR7)	G043H7	Biolegend	353251	**69**	CD95 (Fas)	DX2	Biolegend	305651
25	CD1c	L161	Biolegend	331547	**70**	CX3CR1	K0124E1	Biolegend	355705
26	CD1d	51.1	Biolegend	350319	**71**	HLA-DR	L243	Biolegend	307663
27	CD20	2H7	Biolegend	302363	**72**	IgD	IA6-2	Biolegend	348245
28	CD206 (MMR)	15-2	Biolegend	321147	**73**	IgG	M1310G05	Biolegend	410727
29	CD209 (DC-SIGN)	9E9A8	Biolegend	330121	**74**	IgM	MHM-88	Biolegend	314547
30	CD21	Bu32	Biolegend	354923	**75**	Ig light chain κ	MHK-49	Biolegend	316533
31	CD23	EBVCS-5	Biolegend	338525	**76**	Ig light chain λ	MHL-38	Biolegend	316629
32	CD24	ML5	Biolegend	311143	**77**	Siglec-8	7C9	Biolegend	347115
33	CD25	BC96	Biolegend	302649	**78**	TCR Vα7.2	3C10	Biolegend	351735
34	CD269 (BCMA)	19F2	Biolegend	357523	**79**	TCR γ/δ	B1	Biolegend	331231
35	CD27	O323	Biolegend	302853	**80**	TIGIT (VSTM3)	A15153G	Biolegend	372729
36	CD274 (PD-L1)	29E.2A3	Biolegend	329751	**81**	XCR1	S15046E	Biolegend	372617
37	CD275 (ICOSL)	2D3	Biolegend	309419		***Custom oligo-conjugated in-house***			
38	CD279 (PD-1)	EH12.2H7	Biolegend	329963	**82**	ACE2	535919	Sino Biological	MAB9332-100
39	CD28	CD28.2	Biolegend	302963	**83**	CD160	BY55	Biolegend	341202
40	CD29 (Integrin β1)	TS2/16	Biolegend	303029	**84**	CD16b	2D2G5B9	Sino Biological	11046-MM01
41	CD3	UCHT1	Biolegend	300479	**85**	CD178	NOK-1	Biolegend	306402
42	CD307d (FcRL4)	413D12	Biolegend	340213	**86**	CD34	581	Biolegend	343602
43	CD307e (FcRL5)	509f6	Biolegend	340309	**87**	CD43	CD43-10G7	Biolegend	343202
44	CD309 (VEGFR2)	7D4-6	Biolegend	359921	**88**	CD9	HI9a	Biolegend	312102
45	CD32 (FcγRII)	FUN-2	Biolegend	303225	**89**	IgA	IS11-8E10	Myltenyi	130-093-073

Extended Data Table 5. ***Panel of oligo-conjugated antibodies used in multi-omics scRNA-seq assays to measure surface protein markers on cells from airways and blood.*** A total of 89 oligo-conjugated antibody-derived tags (ADT) were used to evaluate surface protein expression of target antigens via scRNA-seq. Reagents no. 82-89 were not commercially available in the TotalSeq-C™ format (BioLegend), so custom oligo-conjugated reagents were generated in-house using purified monoclonal antibodies and commercially available 5' Feature Barcode Antibody Conjugation - Lightning-Link® kits (abcam). Titrations of all reagents were determined in-house for each lot independently prior to use. Cells were surface stained prior to encapsulation and surface marker expression of major lineage markers were used to help cluster/validate gene expression data as described in the methods.

		PID	Total reads	Mean reads/cell
ETA	GEX	PHA0007	593,835,060	350,345
		PHA0008	555,825,992	2,241,234
		PHA0010	587,153,474	872,442
		PHA0018	541,561,148	459,729
	ADT	PHA0007	85,070,531	2,101
		PHA0008	78,647,311	7,514
		PHA0010	46,042,783	2,989
		PHA0018	73,265,461	5,399
Blood	GEX	PHA0007	518,672,044	273,129
		PHA0008	540,400,013	641,044
		PHA0010	592,394,112	543,980
		PHA0018	556,699,985	1,484,533
		PHA1005	541,306,254	158,787
		PHA1006	501,896,927	200,198
		PHA1007	512,999,099	172,902
		PHA1008	506,988,059	160,898
		PHA1009	527,201,752	130,463
		PHA1010	480,796,663	332,042
	ADT	PHA0007	74,597,277	2,115
		PHA0008	80,175,737	1,536
		PHA0010	62,927,249	1,067
		PHA0018	79,818,668	1,395
		PHA1005	77,435,258	1,145
		PHA1006	88,850,369	1,334
		PHA1007	88,329,209	1,169
		PHA1008	93,579,790	1,351
		PHA1009	91,162,676	1,281
		PHA1010	89,597,131	1,251

Extended Data Table 6. ***Sequencing depth of independent samples.*** All gene expression (GEX) libraries were pooled and run in a single S4 flow cell on a NovaSeq™ 6000. All antibody-derived tag (ADT) libraries were pooled and sequenced in a single lane of a S4 flow cell on a NovaSeq™ 6000. Total reads and mean number of reads per cell for GEX and ADT are reported independently for each sample, with an average read depth of 540,000,000 reads per sample (GEX) and 79,000,000 reads per sample (ADT).

a

PID	Blood (%)	ETA (%)
PHA0007	30	30
PHA0008	20	25
PHA0010	10	25
PHA0018	30	25
PHA1005	30	
PHA1006	30	
PHA1007	30	
PHA1008	20	
PHA1009	20	
PHA1010	25	

b

	Total ADT UMI	
PID	**Blood**	**ETA**
PHA0007	125–500	125–1250
PHA0008	125–1000	125–1250
PHA0010	125–1500	125–750
PHA0018	125–1500	125–1000
PHA1005	125–1250	
PHA1006	125–1250	
PHA1007	125–1500	
PHA1008	125–1500	
PHA1009	125–1500	
PHA1010	125–1500	

Extended Data Table 7. ***Mitochondrial gene thresholds and total ADT UMIs of individual samples.*** (a)Threshold for mitochondrial gene distribution (percentage) for each sample used to exclude potential dead cells in scRNA-seq data. Threshold was evaluated and set for each sample independently. (b) The distribution of total ADT UMIs was determined and recorded per each sample independently.

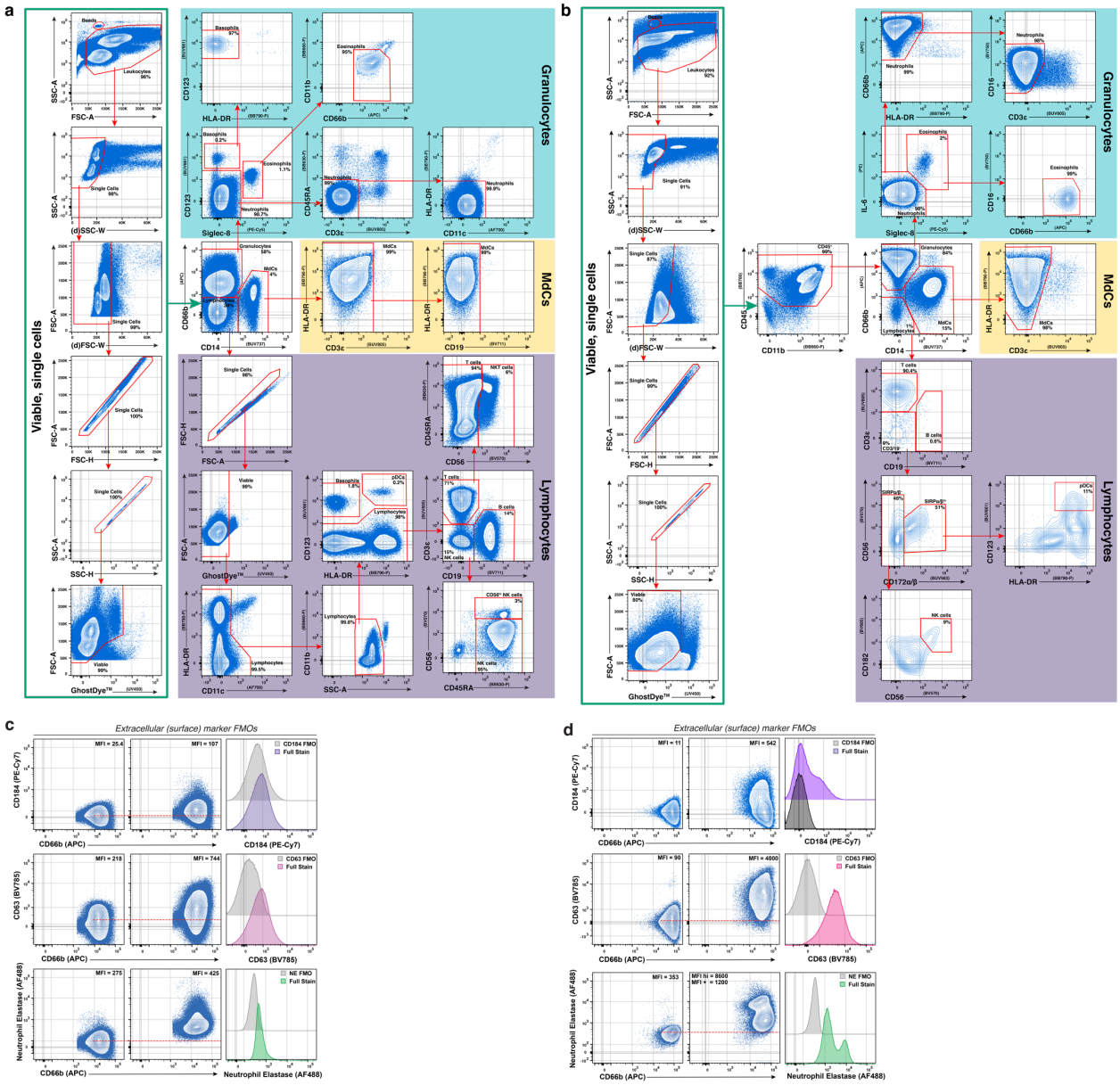

Extended Data Figure 1. ***Representative gating strategy for Hi-D FACS data.*** Representative gating of blood (a) and ETA (b) samples. Extracellular stain FMOs for markers used to interrogate neutrophil phenotype in blood (c) and ETA (d).

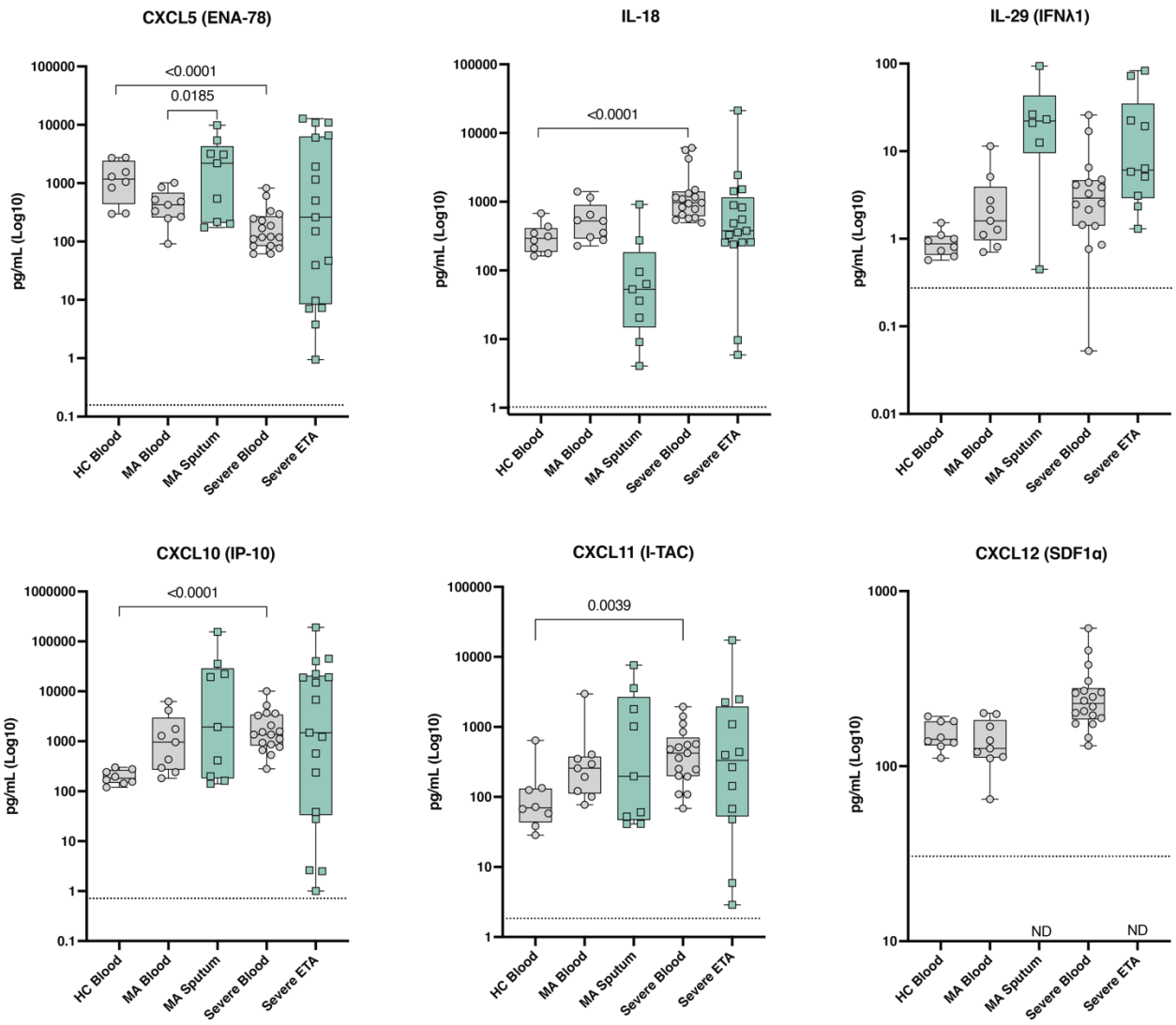

Extended Data Figure 2. ***Additional cytokine assessment in blood and lungs*.** Concentration (pg/mL) of remaining 6 analytes interrogated by Mesoscale analyses in plasma (gray circles) and respiratory supernatant (Resp. SNT; green squares) from healthy control (HC), mild-acute (MA), and severe COVID-19 patients. Dotted line = assay limit of detection (LOD).

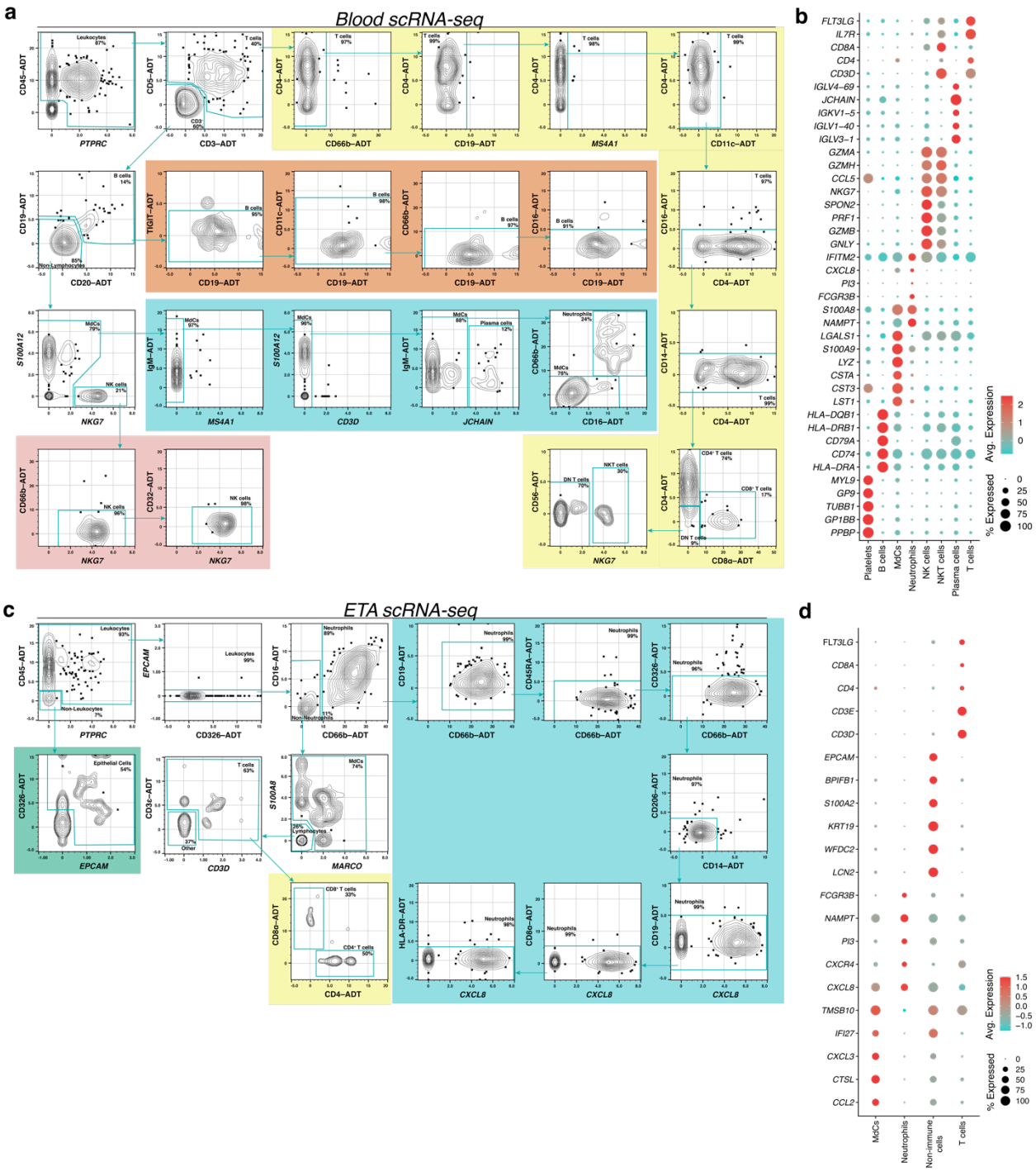

Extended Data Figure 3. ***Multi-omic scRNA-seq analysis of leukocytes in the blood and lung.*** Gating strategy (a and c) employed to classify major lineages of immune cells by surface antibody-derived tag (ADT) and dot plots of the intersection of the top differentially expressed genes sorted by average log-fold change across cell populations (b and d) from the blood (a-b) and ETA (c-d) of severe COVID-19 patients using the SuPPER-seq pipeline previously described[30].

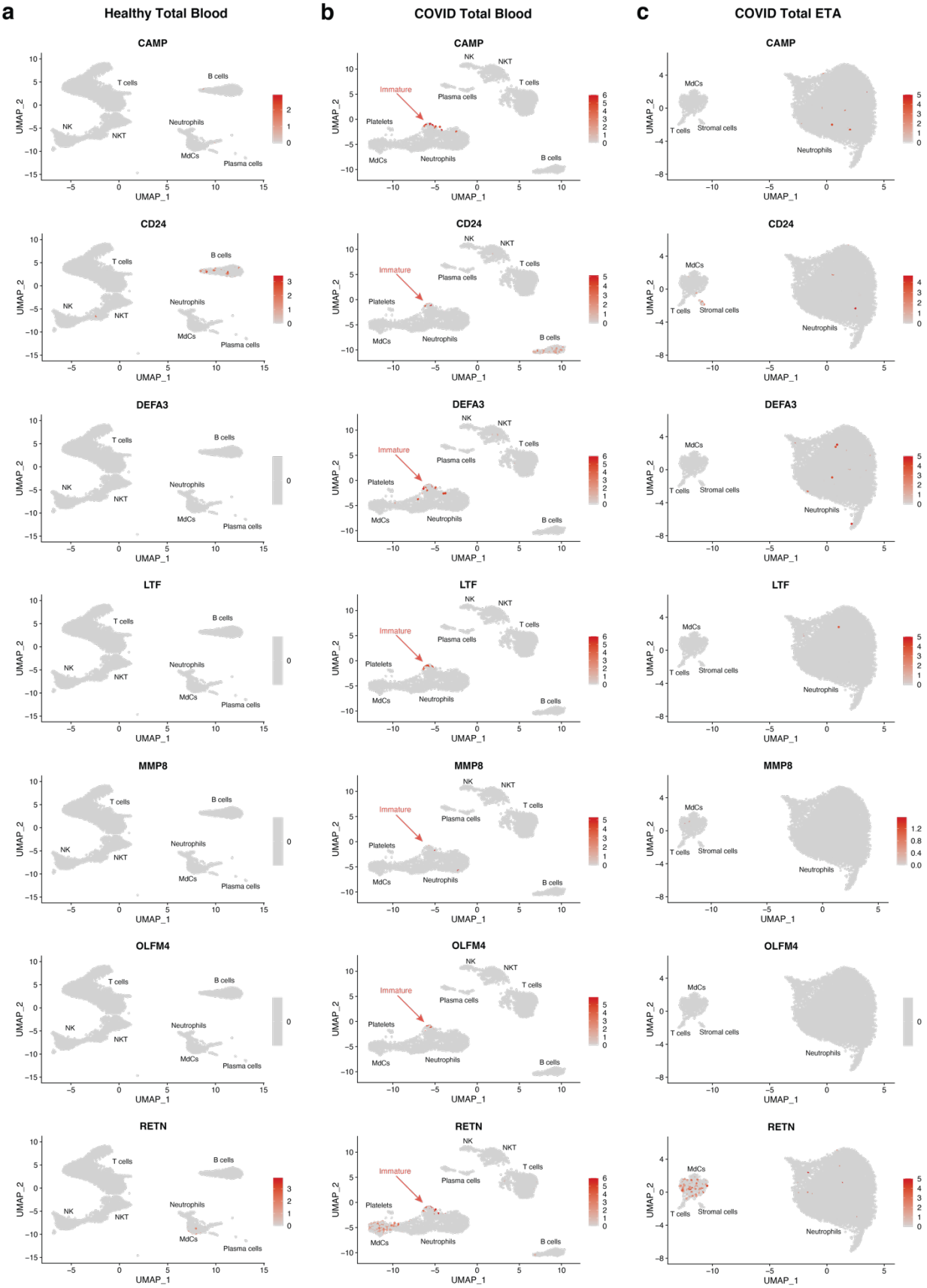
a
Healthy Total Blood
b
COVID Total Blood
c
COVID Total ETA
CAMP
CD24
DEFA3
LTF
MMP8
OLFM4
RETN
UMAP_1
UMAP_2
T cells
B cells
NK
NKT
Neutrophils
MdCs
Plasma cells
Immature
Platelets
Stromal cells

1221

1222 **Extended Data Figure 4.** ***Gene signature for immature neutrophils is lacking in healthy***
1223 ***donors and lungs of COVID-19 patients*****.** UMAP visualizations of genes that identify immature
1224 neutrophils in the blood healthy individuals (a) and severe COVID-19 patients (b), along with
1225 cells from the lungs of severe COVID-19 patients (c).
1226

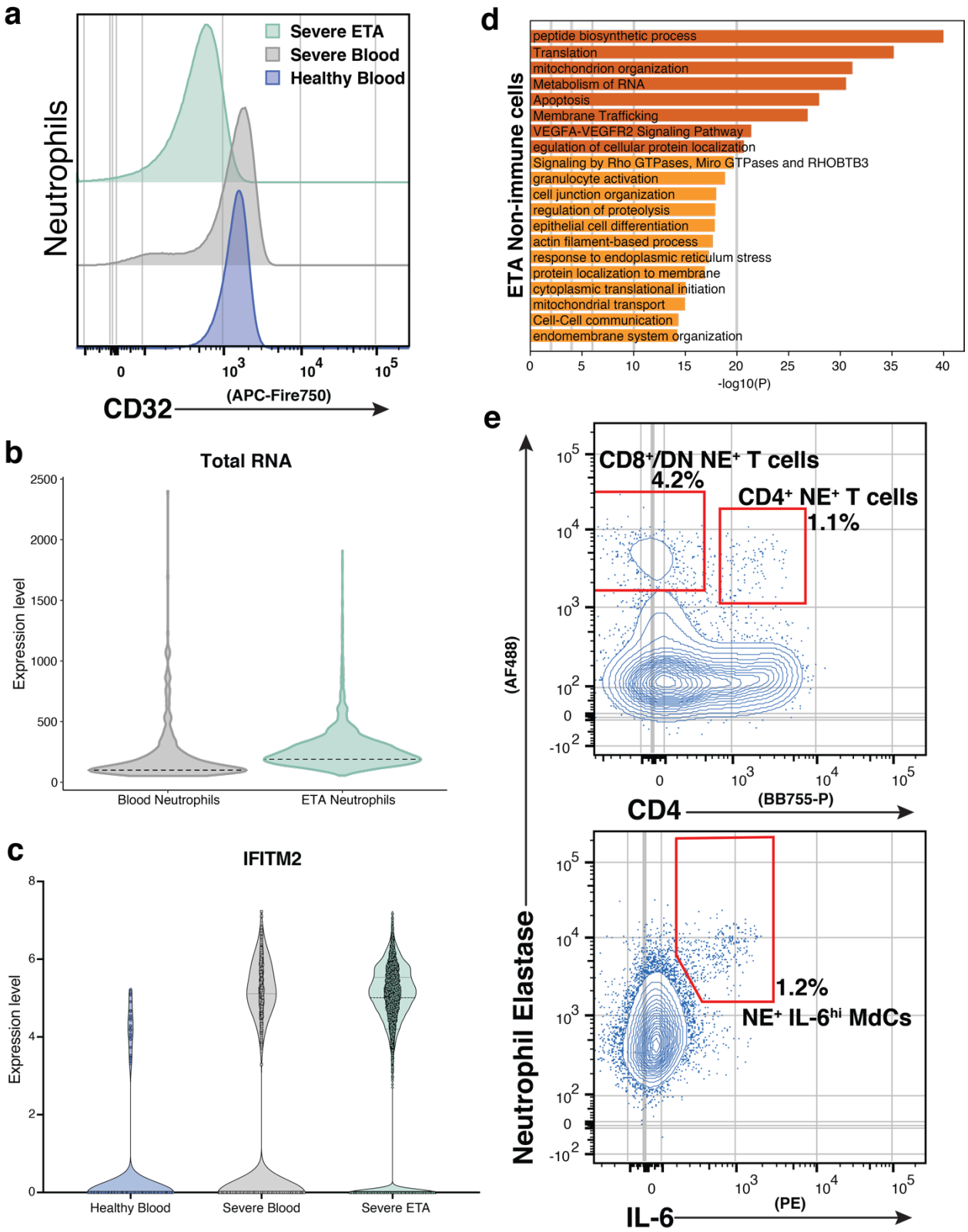

Extended Data Figure 5. ***Cellular signatures during SARS-CoV-2 pathogenesis.*** (a) Pulmonary neutrophils have a reduction in CD32 (FcγRII) expression as compared to circulating

1231 neutrophils. (b) Neutrophils undergo transcriptional reprogramming and increase de novo
1232 transcription (total RNA) upon migrating to the lung. (c) Neutrophils in the blood and lung
1233 increase expression of *IFITM2* during SARS-CoV-2 pathogenesis. (d) Metascape[85] pathway and
1234 process enrichment analyses reveal non-immune cells have an increased gene signature for
1235 granulocyte activation in the airways of severe COVID-19 patients. (e) Extracellular neutrophil
1236 elastase is also detected on the surface of pulmonary T cells and myeloid-derived cells (MdCs)
1237 in severe COVID-19 patients.
1238
1239
1240